

General Disclaimer

One or more of the Following Statements may affect this Document

- This document has been reproduced from the best copy furnished by the organizational source. It is being released in the interest of making available as much information as possible.
- This document may contain data, which exceeds the sheet parameters. It was furnished in this condition by the organizational source and is the best copy available.
- This document may contain tone-on-tone or color graphs, charts and/or pictures, which have been reproduced in black and white.
- This document is paginated as submitted by the original source.
- Portions of this document are not fully legible due to the historical nature of some of the material. However, it is the best reproduction available from the original submission.

N O T I C E

THIS DOCUMENT HAS BEEN REPRODUCED FROM
MICROFICHE. ALTHOUGH IT IS RECOGNIZED THAT
CERTAIN PORTIONS ARE ILLEGIBLE, IT IS BEING RELEASED
IN THE INTEREST OF MAKING AVAILABLE AS MUCH
INFORMATION AS POSSIBLE



PSU/TURBO R81-7

SEMI-ANNUAL PROGRESS REPORT ON
END WALL FLOWS IN ROTORS AND STATORS
OF A SINGLE STAGE COMPRESSOR

T. R. GOVINDAN, B. LAKSHMINARAYANA, A. PANDYA, AND M. POUAGARE

NASA GRANT NSG 3212
NATIONAL AERONAUTICS & SPACE ADMINISTRATION
LEWIS RESEARCH CENTER

(NASA-CR-164635) END WALL FLOWS IN ROTORS AND STATORS OF A SINGLE STAGE COMPRESSOR
Semiannual Progress Report (Pennsylvania State Univ.) 50 p HC A03/MF A01 CACL 21E N81-28097
Unclass 31396
G3/07

TURBOMACHINERY LABORATORY
DEPARTMENT OF AEROSPACE ENGINEERING
THE PENNSYLVANIA STATE UNIVERSITY
UNIVERSITY PARK, PA 16802

AUGUST 1981



**Semi-Annual Progress Report on
END WALL FLOWS IN ROTORS AND STATORS
OF A SINGLE STAGE COMPRESSOR**

(NASA Grant 3212)

by

T. R. Govindan, B. Lakshminarayana, A. Fandya, and M. Pouagare

Submitted to

**National Aeronautics and Space Administration
Lewis Research Center
21000 Brookpark Road
Cleveland, Ohio**

(Grant Monitor - P. Sockol)

**Department of Aerospace Engineering
The Pennsylvania State University
University Park, PA 16802**

August 1981

PREFACE

A brief summary of the research carried out under the NASA Grant NSG 3212 during the six month period ending June 30, 1981, is described in this report. The authorship is quoted in alphabetical order.

T. R. Govindan is responsible for end wall flow analysis, A. Pandya has carried out the leakage flow measurement, and M. Pouagare carried out the hub wall flow measurement.

An M.S. thesis by A. Pandya is in preparation and will be sent out before the next reporting period.

TABLE OF CONTENTS

| | <u>Page</u> |
|---|-------------|
| PREFACE | ii |
| NOMENCLATURE | iv |
| CHAPTER | |
| 1 Solution of the Flow in the Rotor End Wall Region, Including the Effects of Tip-Clearance Flow | 1 |
| 1.1 Introduction | 1 |
| 1.2 The Equations | 2 |
| 1.3 Numerical Scheme | 3 |
| 1.4 Status of the Program | 7 |
| 2 Leakage Flow Measurement at the Tip of a Compressor Rotor Blade | 8 |
| 2.1 Clearance Measurements | 8 |
| 2.2 Flowfield Measurements | 8 |
| 2.3 Results | 12 |
| 3 Measurements of the Rotor Hub Wall Boundary Layer | 14 |
| 4 Publications and Presentations | 16 |
| REFERENCES | 17 |
| APPENDIX I. The Flux Vectors and Jacobian Matrices | 18 |

NOMENCLATURE

| | |
|------------------|--|
| c | chord length |
| $C_{P_{static}}$ | $(\bar{P} - P_{reference})/D$ |
| $C_{P_{total}}$ | $(P_5 - P_{T_{reference}})/D$ |
| $C_{P_{pitch}}$ | $(P_3 - P_4)/D$ |
| $C_{P_{yaw}}$ | $(P_1 - P_2)/D$ |
| d | diameter of the probe head |
| D | $P_5 - \bar{P}$ |
| e | internal energy |
| h | height of the probe from the wall |
| p | static pressure |
| \bar{P} | $(P_1 + P_2 + P_3 + P_4)/4$ |
| P_i | $i = 1 \dots 5$ pressures indicated by five-hole probe tubes (Fig. 11) |
| Q_1 | inlet total relative velocity |
| r, θ, z | cylindrical coordinate system |
| R | r/r_t |
| R_e | Reynolds number |
| w, v, u | velocities in radial, tangential, and axial directions, respectively |
| α | absolute flow angle measured from the axial direction |
| γ | ratio of specific heats |
| μ | viscosity |
| ξ, η, r | transformed coordinates in the streamwise, normal, and radial directions, respectively |
| ρ | density |
| Ω | angular velocity |

Subscripts

t,h values at the tip and hub, respectively

m maximum value

r,θ,z values in the radial, tangential, and axial directions,
respectively

T total

1. SOLUTION OF THE FLOW IN THE ROTOR END WALL REGION, INCLUDING THE EFFECTS OF TIP-CLEARANCE FLOW

1.1 Introduction

The end-wall boundary layer in a rotor blade row is one of the more complicated aspects of the flow in turbomachinery. The flow is three-dimensional and both the radial and tangential gradients of flow variables are important. However, since this is a flow with a dominant flow direction, the streamwise diffusion terms in the Navier-Stokes equations can be neglected in comparison to the diffusion in the radial and tangential directions. This renders the equations parabolic and amenable to solution by a marching procedure.

An important part of the endwall flow phenomenon is the effect of blade tip clearance. Any prediction scheme of the flow in this region must take this effect into consideration. Figure 1 shows the flow domain of interest and its relation to flow in the rotor. It is immediately noticed that the effect of tip clearance on the solution of the flow in the domain is through the boundary conditions prescribed along AB and FE (Figure 1). The choice of AB and FE as boundaries of the domain is dictated by the nature of the flow and convenience, since it is obvious that these lines are neither physical boundaries nor are they lines of periodicity. However, it would seem that the flow in the region A'B'BA can be described by simple flow equations based on the pressure drop across the pressure and suction surfaces of the blade and simple modelling of the viscous terms, for the flow normal to the streamwise direction. Limited experimental evidence suggests that this is the dominant flow direction in the region. In such a situation,

the parameter that couples the solutions to the end-wall and tip-clearance flows is the pressure drop. This is very convenient from the point of view of the solution scheme (to be described in later sections) for the end wall flow where a global pressure iteration is used to update the pressure field. For every one of these iterations, the tip clearance flow can be updated using the newly calculated pressure distribution, and the boundary conditions along AB and FE modified before proceeding to the next pressure iteration.

Consequently, the first and important part of the solution procedure would be the solution of the flow in the region ACDF. The equations and the method of solution are described in the next section.

1.2 The Equations

The Navier-Stokes equations in a rotating cylindrical coordinate system can be written in the form

$$\frac{\partial E}{\partial z} + \frac{\partial F}{\partial \theta} + \frac{\partial G}{\partial r} + C = \frac{1}{Re} \left[\frac{\partial P}{\partial r} + \frac{\partial Q}{\partial \theta} + \frac{\partial T}{\partial z} + S \right] \quad (1)$$

The terms that constitute the vectors E, F, G, C, P, Q, T, S are described in Appendix I. The choice of a cylindrical coordinate instead of a Cartesian system was dictated by a simpler grid generation scheme in the former case. Two dimensional grids can be stacked in the radial direction in preference to the complication of generating three dimensional grids. The equations are transformed to a body fitted coordinate system and the flow domain mapped to a sector of a cylinder in which the computations are carried out. This transformation can be described as

$$\xi \equiv \xi(z, \theta)$$

$$\eta \equiv \eta(z, \theta)$$

$$r \equiv r$$

where ξ is the coordinate on the body surface in the streamwise direction and η normal to it on the cylindrical surface of radius r .

The diffusion terms in the ξ direction can be dropped to make the equations parabolic in this direction and amenable to solutions by a marching procedure. It can easily be shown that the form of the transformed equation can be kept similar to equation (1)

$$\frac{\partial \hat{E}}{\partial \xi} + \frac{\partial \hat{F}}{\partial \eta} + \frac{\partial \hat{G}}{\partial r} + \hat{C} = \frac{1}{Re} \left[\frac{\partial \hat{P}}{\partial r} + \frac{\partial \hat{Q}}{\partial \eta} + \hat{S} \right] \quad (2)$$

where

$$\hat{E} = \xi_z E + \xi_\theta F$$

$$\hat{F} = \xi_z E + \xi_\theta F$$

and

$$\hat{G} \equiv G$$

$$\hat{C} \equiv C$$

$$\hat{P} \equiv P$$

$$\hat{S} \equiv S$$

remain unchanged in the transformation. The terms that constitute the above vectors are described in Appendix I. Equation (2) describes the flow in the computational domain and is the basis for the numerical solution procedure described next.

1.3 Numerical Scheme

The numerical scheme to be described is based on the Linearized Block Implicit Method of Briley and McDonald [1]. This procedure was chosen in favor of the delta scheme of Beam and Warming in that it provided more

versatility in configuring the scheme for the form of the equation described by equation (2). Further, the scheme is consistent in its intermediate steps allowing physical boundary conditions to be applied. Unlike in a time-marching method where only the final steady solution is important, this scheme must march along a spatial direction and every step describes the development of the flow in the streamwise direction.

For the purpose of describing the numerical algorithm, equation (2) can be written in a simpler form as

$$\frac{\partial H(q)}{\partial \xi} = D(q) + \hat{S}(q) \quad (3)$$

where

$$\begin{aligned} H(q) &= \hat{E}(q) \\ D(q) &= \frac{1}{Re} \left[\frac{\partial \hat{P}}{\partial r} + \frac{\partial \hat{Q}}{\partial \eta} \right] - \frac{\partial \hat{F}}{\partial \eta} - \frac{\partial \hat{G}}{\partial r} \\ \hat{S}(q) &= S(q) - C(q) \end{aligned}$$

$D(q)$ contains the spatial derivative terms and is multi-dimensional, q is vector of dependent variables, and $\hat{S}(q)$ is a column vector dependent on q . ξ is the time-like coordinate and (η, r) are the spatial coordinates. We can write a second order accurate finite difference equivalent to (2) in the form

$$(H^{n+1} - H^n)/\Delta \xi = \beta [D(q) + \hat{S}(q)]^{n+1} + (1 - \beta) [D(q) + \hat{S}(q)]^n \quad (4)$$

when $\beta = 1/2$ we have the Crank-Nicolson scheme. The system of equations described by equation (4) is still non-linear and needs to be linearized as follows:

$$\begin{aligned}
H^{n+1} &= H^n + \left(\frac{\partial H}{\partial q}\right)^n (q^{n+1} - q^n) + O(\Delta\xi)^2 \\
\hat{S}^{n+1} &= \hat{S}^n + \left(\frac{\partial \hat{S}}{\partial q}\right)^n (q^{n+1} - q^n) + O(\Delta\xi)^2 \\
D^{n+1} &= D^n + \left(\frac{\partial D}{\partial q}\right)^n (q^{n+1} - q^n) + O(\Delta\xi)^2
\end{aligned} \tag{5}$$

The linearized scheme is then given by,

$$\left(\frac{\partial H^n}{\partial q}\right) (q^{n+1} - q^n) / \Delta\xi = D^n + \hat{S}^n + \beta \left(\frac{\partial D}{\partial q} + \frac{\partial \hat{S}}{\partial q}\right) (q^{n+1} - q^n)$$

or

$$(A + \Delta\xi L)\psi^{n+1} = \Delta\xi [D(q)^n + \hat{S}^n]$$

where

$$A = \frac{\partial H^n}{\partial q} - \beta \Delta\xi \left(\frac{\partial \hat{S}^n}{\partial q}\right)$$

$$L = -\beta \frac{\partial D}{\partial q}$$

and

$$\psi^{n+1} = q^{n+1} - q^n$$

Expanding the operators into their multi-dimensional form

$$[A + \Delta\xi (L_\eta + L_\tau)]\psi^{n+1} = \Delta\xi [(D_\eta + D_\tau)q^n + \hat{S}^n]$$

Factorising the scheme based on the Douglas-Gunn split, we have

$$[A + \Delta\xi L_\eta]\psi^* = \Delta\xi [(D_\eta + D_\tau)q^n + \hat{S}^n]$$

$$[A + \Delta\xi L_\tau]\psi^{**} = A\psi^* \tag{6}$$

$$\psi^{n+1} = \psi^{**}$$

The difference scheme is of order $(\Delta\xi)^2$ and is consistent at its intermediate step. It should be noted that in writing the above factorized scheme, mixed derivative terms occurring in the Jacobian matrices of L need to be explicitly differenced to keep the system of algebraic equations describing the discretization of equations (6) block tridiagonal. As has been shown by Beam and Warming [2], this does not impair the stability or accuracy of the scheme.

It must be noted that the general solution to the equation (3) would allow an exponential term that would grow if an eigenvalue of the Jacobian matrix of H, $\partial H/\partial q$, is negative. As has been shown by Schiff and Steger [3], this is indeed true for subsonic flow. Details of the analysis are in [3] and are not included here for brevity. This condition is to be expected from the known elliptic nature of the pressure field. Schiff and Steger show that the eigenvalues can all be made positive by removing the pressure dependency from the Jacobian matrix $\partial H/\partial q$. The eigenvalues are positive provided the streamwise velocity is positive, restricting the method to unseparated flows. This, again, is an expected result.

To remove the dependency of the Jacobian matrix of H on the pressure requires the specification that $p \neq p(q)$ i.e., the pressure field must be specified in the marching equations. A global pressure iteration must be implemented to converge the solution. To begin with, the boundary layer approximation, $\partial p/\partial r = 0$ is used and the pressure field equated to that in the outer inviscid flow. On marching the solution a new pressure field is obtained that is used to update the specified pressure field. This is the technique of global pressure iteration.

As mentioned in a previous section, the global pressure iteration can also be used to update the tip-clearance flow solution. The new pressure

field is used to predict a new tip clearance flow solution that modifies the boundary conditions to the end-wall boundary layer equations.

1.4 Status of the Program

A computer program has been written to implement the solution procedure just described. Initial debugging of the code is complete. The present version is configured for a maximum 50 x 50 grid size, runs on The Pennsylvania State University's IBM 3033/370 processor using the Fortran H-extended compiler. Run times per marching step are of the order of two seconds for a 20 x 20 grid. This run time includes I/O time used for disk I/O operations.

Further reductions in this time should be expected in final versions of the code.

The code is currently being used to predict the flow in a 90° bend using the experimental data of Taylor et al. [4]. Preliminary results are encouraging.

2. LEAKAGE FLOW MEASUREMENT AT THE TIP OF A COMPRESSOR ROTOR BLADE

Detailed hot wire measurements inside the clearance region of the Axial Flow Compressor Rotor in the Department of Aerospace Engineering was undertaken recently. The rotor was operated at the design flow coefficient as well as one off-design flow condition. The probe employed and the schematic of the probe set up are shown in Figures 2 and 3, respectively.

2.1 Clearance Measurements

Instantaneous clearance during the motion of the rotor was found using a fonic sensor, and these measurements were compared with the static clearance for one blade. This process was repeated for four different blades and no appreciable difference was found between the static and the dynamic clearances in all the four cases. Therefore, it was assumed that the clearance did not vary with the rotational speed of the compressor and static clearance measurements were carried out for all the 21 blades at various axial locations. Table 1 shows the clearance in thousands of an inch at five axial locations.

2.2 Flowfield Measurements

Flowfield measurements inside the clearance region and the rotor exit in the end wall region were carried out using a stationary "v" configuration hot-wire probe in combination with ensemble averaging technique.

Figure 2 shows the two sensor hot wire probe used for these measurements. Unlike the conventional two sensor probes (x configuration), this probe has both the sensors in the same plane and are at right angles to each other.

Table 1. Clearance in Thousands of an Inch at Various Axial Stations

| Blade # | Z = 0.00 | Z = 0.25 | Z = 0.50 | Z = 0.75 | Z = 0.979 |
|---------|----------|----------|----------|----------|-----------|
| 1 | 95 | 76 | 74 | 65 | 61 |
| 2 | 96 | 78 | 72 | 66 | 63 |
| 3 | 99 | 79 | 74 | 69 | 67 |
| 4 | 99 | 80 | 76 | 68 | 63 |
| 5 | 99 | 81 | 76 | 68 | 62 |
| 6 | 96 | 79 | 79 | 65 | 61 |
| 7 | 100 | 83 | 76 | 67 | 62 |
| 8 | 98 | 78 | 73 | 65 | 64 |
| 9 | 92 | 78 | 74 | 66 | 66 |
| 10 | 100 | 78 | 73 | 64 | 63 |
| 11 | 100 | 80 | 74 | 66 | 62 |
| 12 | 97 | 76 | 71 | 63 | 60 |
| 13 | 95 | 78 | 72 | 64 | 64 |
| 14 | 100 | 78 | 73 | 62 | 59 |
| 15 | 86 | 77 | 73 | 59 | 57 |
| 16 | 85 | 74 | 73 | 56 | 56 |
| 17 | 92 | 77 | 65 | 60 | 56 |
| 18 | -- | 80 | 70 | 60 | 52 |
| 19 | -- | 81 | 72 | 61 | 51 |
| 20 | 104 | 80 | 74 | 64 | 57 |
| 21 | 101 | 80 | 74 | 63 | 59 |

The probe was introduced in the flow field through the holes made at several axial locations on the lucite window. Care was taken to avoid a sudden step (and thereby generation of eddies) at the location where the probe was introduced. Figure 3 shows the arrangement made to avoid the step. Figure 4 shows the schematic of the instrumentation used for the hot wire measurements and data processing.

The sensors were connected to two DISA 55M10 constant temperature anemometer units. The d.c. components of the anemometer signals were measured with an integral digital voltmeter. The fluctuating components of these signals were amplified and recorded with SAVRE IV FM signal recorder/reproducer at the tape speed of 15 i.p.s.

The r.p.m. of the rotor was monitored by a photo cell circuit which used a 60 slot calibrated disk mounted on the rotor shaft. The output of the photocell circuit was displayed on a digital counter. The photocell circuit also provided one sharp pulse for each revolution of the rotor. This pulse was also recorded along with the a.c. signals to identify a specific blade passage.

The instantaneous signals from the anemometer and the pulse were displayed on Tektronix type RM561A storage oscilloscope.

Measurements were taken at five axial locations for tip leakage flow and four locations for rotor exit flow. Rotor inlet flow was measured at one location 1/8 in. upstream of the leading edge. The axial and radial locations at which the measurements were taken are listed in Table 2. At each axial location, the probe was traversed as near the blade as possible (0.010 in. away from the blade tip with minimum clearance) without damaging the probe. The probe was traversed at an interval .005 in. The same procedure was repeated for the measurements at the off design conditions.

Table 2. Axial and Radial Locations for Flow Field Measurements

| z/c | τ | | 10 | 15 | 20 | 25 | 30 | 35 | 40 | 45 | 50 | 60 | 75 | 100 | 125 | 150 | 175 | 180 | 80 | |
|-------|--------------|--------------|----|----|----|----|----|----|----|----|----|----|----|-----|-----|-----|-----|-----|----|---|
| | $\phi = .55$ | $\phi = .60$ | * | * | * | * | * | * | * | * | * | * | * | * | * | * | * | * | * | * |
| 0.00 | $\phi = .55$ | * | * | * | * | * | * | * | * | * | * | * | * | * | * | * | * | * | * | * |
| | $\phi = .60$ | * | * | * | * | * | * | * | * | * | * | * | * | * | * | * | * | * | * | * |
| 0.25 | $\phi = .55$ | * | * | * | * | * | * | * | * | * | * | * | * | * | * | * | * | * | * | * |
| | $\phi = .60$ | * | * | * | * | * | * | * | * | * | * | * | * | * | * | * | * | * | * | * |
| 0.50 | $\phi = .55$ | * | * | * | * | * | * | * | * | * | * | * | * | * | * | * | * | * | * | * |
| | $\phi = .60$ | * | * | * | * | * | * | * | * | * | * | * | * | * | * | * | * | * | * | * |
| 0.75 | $\phi = .55$ | * | * | * | * | * | * | * | * | * | * | * | * | * | * | * | * | * | * | * |
| | $\phi = .60$ | * | * | * | * | * | * | * | * | * | * | * | * | * | * | * | * | * | * | * |
| 0.979 | $\phi = .55$ | * | * | * | * | * | * | * | * | * | * | * | * | * | * | * | * | * | * | * |
| | $\phi = .60$ | * | * | * | * | * | * | * | * | * | * | * | * | * | * | * | * | * | * | * |
| 0.021 | $\phi = .55$ | * | * | * | * | * | * | * | * | * | * | * | * | * | * | * | * | * | * | * |
| | $\phi = .60$ | * | * | * | * | * | * | * | * | * | * | * | * | * | * | * | * | * | * | * |
| 0.41 | $\phi = .55$ | * | * | * | * | * | * | * | * | * | * | * | * | * | * | * | * | * | * | * |
| | $\phi = .60$ | * | * | * | * | * | * | * | * | * | * | * | * | * | * | * | * | * | * | * |
| 0.125 | $\phi = .55$ | * | * | * | * | * | * | * | * | * | * | * | * | * | * | * | * | * | * | * |
| | $\phi = .60$ | * | * | * | * | * | * | * | * | * | * | * | * | * | * | * | * | * | * | * |
| 0.450 | $\phi = .55$ | * | * | * | * | * | * | * | * | * | * | * | * | * | * | * | * | * | * | * |
| | $\phi = .60$ | * | * | * | * | * | * | * | * | * | * | * | * | * | * | * | * | * | * | * |

τ is the distance in thousands of an inch from the annulus wall.

* Data acquired
 - Data not acquired

For the rotor exit flow measurements, in the region away from the wall, the probe was traversed at the interval of .025 in. In the region very near the wall the probe was traversed at the interval of .010 in.

Table 3 lists the various parameters at the two operating conditions at which the measurements were carried out.

2.3 Results

The data at $z/c = 0.75$, $\phi = 0.55$ has been processed using the ensemble average technique. All other data will be incorporated and interpreted in the M.S. thesis by A. Pandya.

Figure 5 shows the tangential variation of mean axial velocity for one blade passage. The mean axial velocity was normalized by the local maximum axial velocity. It can be noted from this figure that curves for various radial location collapse into a single curve. Attempts are presently being made to identify the location of gap region in this curve. Figure 6 shows the variation of the mean tangential velocity which is normalized with respect to the local maximum axial velocity. A similar trend is observed as in the case of mean axial velocity i.e., a sharp decrease in the mean tangential velocity and all the curves collapsing into one curve in the clearance region. Figure 7 shows the variation of alpha (α), the angle made by the total velocity with the axis of the rotor. Once again, the clearance region is characterized by a sharp decrease in α . There is a large variation in α (approximately 27 degrees) inside one blade passage. Figures 5, 6, and 7 show a peculiar behavior of the flow in the passage, i.e., two peaks in each of these three quantities. This sort of a behavior may be due to the scraping vortex as well as leakage flow.

Table 3. Compressor Operating Conditions

| R.P.M. | Design Condition | Off-Design Condition |
|------------------------|-------------------------------|--------------------------------|
| | | 1100 |
| Inlet Static Pressure | -5.08 cms of H ₂ O | -4.356 cms of H ₂ O |
| Inlet Velocity (Axial) | 28.37 m/sec | 26.28 m/sec |
| Flow Coefficient | 0.55 | 0.60 |

Figure 8 shows the variation of maximum axial velocity at various radial locations. The actual distance from the casing is normalized with respect to the clearance height. It is evident from the figure that the maximum axial velocity is becoming fairly constant at 1/3 of the passage height (2/3 from the casing). This behavior is in accordance with the expected profile where the velocity reaches a maximum very near the blade tip before reaching zero. Unfortunately, it was not possible to go nearer to the blade tip with the present set-up.

Figures 9 and 10 show the variation of the turbulence intensities in the axial and tangential directions, respectively. These are normalized by the local maximum axial velocity. Both these quantities show a behavior which is very similar to that of the mean quantities. A sudden decrease in the turbulence intensities in the clearance region is observed. Reasons for very peculiar and erratic behavior at the radial station 0.011 in. from the casing are not known at the present time.

3. MEASUREMENTS OF THE ROTOR HUB WALL BOUNDARY LAYER

The flow in the hub region of a rotating blade row is one of the least understood aspects of the flow. A better understanding of the flow phenomena in this region is important for the design of the blade row, reduction of the losses, and improvement of the performance of the compressor. Such measurements are also needed to check flow prediction schemes.

This report presents flow measurements taken near the hub wall inside the rotor passage of the single stage axial flow compressor facility at the Department of Aerospace Engineering. A five-hole probe rotating with the blade row is used to measure the three components of the mean velocity, static and total pressure. The probe is shown in Figures 11 and 12. Measurements were taken at four radial ($r/r_t = 0.51, 0.5136, 0.517, 0.52$) and four axial locations ($z/c = 0.245, 0.45, 0.66, 0.866$) at a flow coefficient equal to 0.555. The results are shown in Figures 13 to 16. It can be seen from the axial component of velocity profile that the thickness of the hub wall boundary layer is very small. The radial location which is nearest to the wall is in the outer region of the boundary layer, although it corresponds to a distance of 0.635 cm (1/4 in.) from the wall. The first measuring station is at a distance of 0.635 cm from the suction surface and the last at a distance of 0.79 cm from the pressure surface. At the first two axial locations no blade boundary layer can be seen, but at $z/c = 0.66$ and $z/c = 0.866$ the outer region of the blade boundary layer on the suction side can be clearly identified.

The measurements show almost zero radial velocity at the first two axial stations. At the last two axial locations radial component of velocity exists. It can be seen that W is stronger in the suction side region than in the pressure side region. This is due to the fact that on the suction

side, the radial velocity induced by the secondary vorticity and the radial component of velocity in the blade boundary layer are in the same direction. The opposite happens on the pressure side.

The whole set of measurements were taken very near the wall, so the "wall vicinity" effects were not small. In order to evaluate this effect, the probe was calibrated with the probe axis parallel to a knife-edge plate in a jet. The probe is moved normal to the plate. The results are shown in Figure 17. All the raw data were corrected accordingly.

4. PUBLICATIONS AND PRESENTATIONS

Thesis

R. Davino (M.S. Thesis, November 1980), "Three Dimensional Mean Flow and Turbulence Characteristics in the Annulus Wall Region of an Axial-Flow Compressor Rotor Blade Passage," Dept. of Aerospace Engineering, The Pennsylvania State University.

Publications

N. Sitaram, B. Lakshminarayana, and A. Ravindranath, "Conventional Probes for the Relative Measurement in a Rotor Blade Passage," J. Engineering for Power, Vol. 103, No. 2, pp. 406-416, April 1981.

R. Davino and B. Lakshminarayana, "Characteristics of Mean Velocity at the Annulus Wall Region, at the Exit of a Turbomachinery Rotor Passage," AIAA Paper 81-0068, 1981 (accepted for publication in AIAA Journal).

R. Davino and B. Lakshminarayana, "Turbulence Characteristics in the Annulus Wall Boundary Layer and Wake Mixing Region of a Compressor Exit," ASME Paper 81-GT-148, 1981 (accepted for publication in J. Engineering for Power).

Presentations

B. Lakshminarayana, "Characteristics of Mean Velocity at the Annulus Wall Region at the Exit of Turbomachinery Rotor Passage," AIAA 19th Aerospace Sciences Meeting, St. Louis, Mo., January 12, 1981.

R. Davino, "Rotor Wake Mixing Effects Downstream of a Compressor Rotor," 26th ASME International Gas Turbine Conference, Houston, Texas, March 11, 1981.

Awards

R. Davino - First Place Award in the Graduate Division of the Mid-Atlantic Region AIAA Student Paper Competition, April 24, 1981. Paper and presentation entitled "Characteristics of the Flow in the Annulus Wall Boundary Layer Region of an Axial Flow Compressor Rotor Passage."

REFERENCES

1. Briley, W. R. and McDonald, H., "On the Structure and Use of Linearized Block Implicit Schemes," J. of Comp. Phys., December 1979.
2. Beam, R. M. and Warming, R. F., "Alternating Direction Implicit Methods for Parabolic Equations with a Mixed Derivative," SIAM J. Sci. Stat. Comput., Vol. 1, No. 1, March 1980.
3. Schiff, L. B. and Steger, J. L., "Numerical Simulation of Steady Supersonic Viscous Flow," AIAA Paper 79-0130, January 1979.
4. Taylor, A. M. K. P., Whitelaw, J. H., and Yianneskis, M., "Measurements of Laminar and Turbulent Flow in a Curved Duct with Thin Inlet Boundary Layers," NASA CR 3367.

Appendix I. The Flux Vectors and Jacobian Matrices

$$q = \begin{bmatrix} \rho \\ \rho u \\ \rho v \\ \rho w \\ e \end{bmatrix} \quad \hat{E} = \begin{bmatrix} \rho v \\ \rho u U + \xi_z p \\ \rho v U + \xi_\theta p \\ \rho w U \\ (e + p)U \end{bmatrix}$$

$$\hat{F} = \begin{bmatrix} \rho v \\ \rho u V + \eta_z p \\ \rho v V + \eta_\theta p \\ \rho w V \\ (e + p)V \end{bmatrix} \quad \hat{G} = \begin{bmatrix} \rho w \\ \rho u w \\ \rho v w \\ \rho w^2 + p \\ (e + p)w \end{bmatrix}$$

$$\hat{C} = \begin{bmatrix} \frac{\rho w}{r} \\ \frac{\rho u w}{r} - \rho \Omega^2 R \frac{\partial R}{\partial z} \\ \frac{2\rho v w}{r} + 2\rho \Omega w \\ \frac{\rho(w^2 - v^2)}{r} - \rho \Omega^2 R \frac{\partial R}{\partial r} - 2\rho \Omega v \\ -\frac{e w}{r} - \rho \Omega^2 R (w \frac{\partial R}{\partial r} + u \frac{\partial R}{\partial z}) \end{bmatrix}$$

$$\hat{P} = \begin{bmatrix} 0 \\ u(\frac{\partial u}{\partial r} + \eta_z \frac{\partial w}{\partial \eta}) \\ u(\eta_\theta \frac{\partial w}{\partial \eta} + r \frac{\partial v}{\partial r} \frac{v}{r}) \\ \frac{4}{3} u \frac{\partial w}{\partial r} - \frac{2}{3} u(\eta_\theta \frac{\partial v}{\partial \eta} + \eta_z \frac{\partial u}{\partial \eta} + \frac{w}{r}) \\ u \left[\frac{1}{2} \frac{\partial}{\partial r} (u^2 + v^2 + w^2) - \frac{v^2}{r} - \frac{2}{3} \frac{w^2}{r} + \eta_\theta \frac{\partial v w}{\partial \eta} + \eta_z \frac{\partial u w}{\partial \eta} \right. \\ \left. - \frac{5w}{3} (\eta_\theta \frac{\partial v}{\partial \eta} + \eta_z \frac{\partial u}{\partial \eta}) \right] \end{bmatrix}$$

$$\hat{Q} = \begin{bmatrix} 0 \\ \mu(\eta_\theta^2 + \eta_z^2) \frac{\partial u}{\partial \eta} + \frac{\mu}{3} \eta_z (\eta_\theta \frac{\partial v}{\partial \eta} + \eta_z \frac{\partial u}{\partial \eta}) - \frac{2}{3} \mu (\frac{\partial w}{\partial r} + \frac{w}{r}) \\ \mu(\eta_\theta^2 + \eta_z^2) \frac{\partial v}{\partial \eta} + \frac{\mu}{3} \eta_\theta (\eta_\theta \frac{\partial v}{\partial \eta} + \eta_z \frac{\partial u}{\partial \eta}) - \frac{2}{3} \mu (\frac{\partial w}{\partial r} + \frac{w}{r}) \\ \mu(\eta_\theta^2 + \eta_z^2) \frac{\partial w}{\partial \eta} + \mu (\eta_\theta r \frac{\partial}{\partial r} \frac{v}{r} + \eta_z \frac{\partial u}{\partial r}) \\ \mu \left[\frac{1}{2} (\eta_\theta^2 + \eta_z^2) \frac{\partial}{\partial \eta} (u^2 + v^2 + w^2) + \frac{1}{6} (\eta_\theta^2 \frac{\partial v}{\partial \eta} + \eta_z^2 \frac{\partial u}{\partial \eta} + 2\eta_\theta \eta_z \frac{\partial uv}{\partial \eta}) \right. \\ \left. + \frac{4}{3} \frac{vw}{r} - \frac{2v}{3} \frac{\partial w}{\partial r} + w \frac{\partial}{\partial r} \frac{v}{r} - \frac{2u}{3} \frac{\partial w}{\partial r} + w \frac{\partial u}{\partial r} \right] \end{bmatrix}$$

$$\hat{S} = \begin{bmatrix} 0 \\ \frac{\mu}{r} (\frac{\partial u}{\partial r} + \eta_z \frac{\partial w}{\partial \eta}) \\ \frac{2\mu}{r} (\eta_\theta \frac{\partial w}{\partial \eta} + r \frac{\partial}{\partial r} \frac{v}{r}) \\ \frac{2\mu}{r} (\frac{\partial w}{\partial r} - \eta_\theta \frac{\partial v}{\partial \eta} - \frac{w}{r}) \\ \frac{\mu}{r} \left[\frac{1}{2} \frac{\partial}{\partial r} (u^2 + v^2 + w^2) - \frac{v^2}{r} - \frac{2}{3} \frac{w^2}{r} + \eta_\theta \frac{\partial vw}{\partial \eta} + \eta_z \frac{\partial uw}{\partial \eta} - \frac{5w}{3} (\eta_\theta \frac{\partial v}{\partial \eta} + \eta_z \frac{\partial u}{\partial \eta}) \right] \end{bmatrix}$$

where

$$U = \xi_z u + \xi_\theta v$$

$$V = \eta_z u + \eta_\theta v$$

To obtain the flux vectors in the untransformed coordinate system, we put $\xi_z = 1$, $\xi_\theta = 0$, $\eta_z = 0$, $\eta_\theta = 1$. In deriving the energy equation, heat transfer terms from the temperature gradient have been neglected to reduce the complexity of the equations. Inclusion of these terms should present no additional difficulty to the solution procedure. The equation of state used to close the system of equations is

$$P/\rho = (\gamma - 1)e_i$$

where
$$e_i = (e/\rho) - 0.5(u^2 + v^2 + w^2)$$

The Jacobian Matrix of the Vector \hat{E}

$$e_{12} = \xi_z$$

$$e_{13} = \xi_\theta$$

$$e_{21} = -\xi_z u^2 - \xi_\theta uv$$

$$e_{22} = 2\xi_z u + \xi_\theta v$$

$$e_{23} = \xi_\theta u$$

$$e_{31} = -\xi_z uv - \xi_\theta v^2$$

$$e_{32} = \xi_z v$$

$$e_{33} = \xi_z u + 2\xi_\theta v$$

$$e_{41} = -\xi_z uv - \xi_\theta vw$$

$$e_{42} = \xi_z w$$

$$e_{43} = \xi_\theta w$$

$$e_{44} = \xi_z u + \xi_\theta v$$

$$e_{51} = -\frac{(e+p)}{\rho} (\xi_z u + \xi_\theta v)$$

$$e_{52} = \xi_z (e+p)/\rho$$

$$e_{53} = \xi_\theta (e+p)/\rho$$

$$e_{55} = (\xi_z u + \xi_\theta v)$$

All other elements of the matrix are zero.

The Jacobian Matrix of the Vector \hat{F}

$$f_{12} = \eta_z$$

$$f_{13} = \eta_\theta$$

$$f_{21} = -\eta_z u^2 - \eta_\theta uv + \eta_z \phi^2$$

$$f_{22} = 2\eta_z u + \eta_\theta v - (\gamma - 1)\eta_z u$$

$$f_{23} = \eta_\theta u - (\gamma - 1)\eta_z v$$

$$f_{24} = -(\gamma - 1)\eta_z w$$

$$f_{25} = \eta_z (\gamma - 1)$$

$$f_{31} = -\eta_z uv - \eta_\theta v^2 + \eta_\theta \phi^2$$

$$f_{32} = \eta_z v - (\gamma - 1)\eta_\theta v$$

$$f_{33} = \eta_z u + 2\eta_\theta v - (\gamma - 1)\eta_\theta v$$

$$f_{34} = -(\gamma - 1)\eta_\theta w$$

$$f_{41} = -\eta_z uw - \eta_\theta vw$$

$$f_{42} = \eta_z w$$

$$f_{43} = \eta_\theta w$$

$$f_{44} = \eta_z u + \eta_\theta v$$

$$f_{51} = (\eta_z u + \eta_\theta v)(2\phi^2 - \gamma e/\rho)$$

$$f_{52} = \eta_z (\gamma e/\rho - \phi^2) - (\gamma - 1) u (\eta_z u + \eta_\theta v)$$

$$f_{53} = \eta_\theta (\gamma e/\rho - \phi^2) - (\gamma - 1) v (\eta_z u + \eta_\theta v)$$

$$f_{55} = \gamma (\eta_z u + \eta_\theta v)$$

All other elements of the matrix are zero.

The Jacobian Matrix of the Vector \hat{G}

$$g_{14} = 1$$

$$g_{21} = -uw$$

$$g_{22} = w$$

$$g_{24} = u$$

$$g_{31} = -vw$$

$$g_{33} = w$$

$$g_{34} = v$$

$$g_{41} = -w^2 + \phi^2$$

$$g_{42} = -(\gamma - 1)u$$

$$g_{43} = -(\gamma - 1)v$$

$$g_{44} = 2w - (\gamma - 1)w$$

$$g_{45} = \gamma - 1$$

$$g_{51} = w(2\phi^2 - \gamma e/\rho)$$

$$g_{52} = -(\gamma - 1)uw$$

$$g_{53} = -(\gamma - 1)vw$$

$$g_{54} = (\gamma e/\rho - \phi^2) - (\gamma - 1)w^2$$

$$g_{55} = \gamma w$$

where $\phi^2 = 0.5(\gamma - 1)(u^2 + v^2 + w^2)$

All other elements of the matrix are zero.

The Jacobian Matrix of the Vector C

$$c_{14} = \frac{1}{r}$$

$$c_{21} = -\frac{uw}{r} - \Omega^2 R \frac{\partial R}{\partial z}$$

$$c_{22} = \frac{w}{r}$$

$$c_{24} = \frac{u}{r}$$

$$c_{31} = -\frac{2}{r} vw$$

$$c_{33} = \frac{2w}{r}$$

$$c_{34} = \frac{2v}{r} + 2\Omega$$

$$c_{41} = -\frac{(w^2 - v^2)}{r} - \Omega^2 R \frac{\partial R}{\partial r}$$

$$c_{42} = \frac{2v}{r}$$

$$c_{43} = -\frac{2v}{r} - 2\Omega$$

$$c_{51} = \frac{ew}{\rho r}$$

$$c_{52} = -\Omega^2 R \frac{\partial R}{\partial z}$$

$$c_{54} = \left(-\frac{e}{\rho r} - \Omega^2 R \frac{\partial R}{\partial r}\right)$$

$$c_{55} = -\frac{w}{r}$$

All other elements of the matrix are zero.

The Jacobian Matrix of the Vector \hat{P}

$$P_{21} = -\mu \{D_r \left(\frac{u}{\rho}\right) + \eta_z D_\eta \left(\frac{w}{\rho}\right)\}$$

$$P_{22} = \mu D_r \left(\frac{1}{\rho}\right)$$

$$P_{24} = \mu \eta_z D_\eta \left(\frac{1}{\rho}\right)$$

$$P_{31} = -\mu \{ \eta_\theta D_\eta \left(\frac{w}{\rho}\right) + D_r \left(\frac{v}{\rho}\right) + \frac{v}{\rho r} \}$$

$$P_{41} = -\frac{4}{3} \mu D_r \left(\frac{w}{\rho}\right) + \frac{2}{3} \mu \{ \eta_\theta D_\eta \left(\frac{v}{\rho}\right) + \eta_z D_\eta \left(\frac{u}{\rho}\right) + \frac{w}{\rho r} \}$$

$$P_{33} = \mu \{ D_r \left(\frac{1}{\rho}\right) - \frac{1}{r\rho} \}$$

$$P_{34} = \mu \eta_\theta D_\eta \left(\frac{1}{\rho}\right)$$

$$P_{42} = -\frac{2}{3} \mu \eta_z D_\eta \left(\frac{1}{\rho}\right)$$

$$P_{43} = -\frac{2}{3} \mu \eta_\theta D_\eta \left(\frac{1}{\rho}\right)$$

$$P_{44} = \frac{4}{3} \mu D_r \left(\frac{1}{\rho}\right) - \frac{2}{3} \frac{u}{r\rho}$$

$$P_{51} = \mu \left[-D_r (u^2 + v^2 + 1.333 w^2) / \rho + \frac{2v^2}{\rho r} + \frac{4w^2}{3\rho r} - 2\eta_\theta D_\eta \left(\frac{vw}{\rho}\right) - \eta_z \frac{2uw}{\rho} \right. \\ \left. + \frac{5w}{3} \eta_\theta D_\eta \frac{v}{\rho} + \frac{5}{3} \eta_\theta \frac{w}{\rho} \frac{\partial v}{\partial \eta} + \frac{5w}{3} \eta_z D_\eta \frac{u}{\rho} + \frac{5}{3} \eta_z \frac{u}{\rho} \frac{\partial u}{\partial \eta} \right]$$

$$P_{52} = \mu \left[D_r \frac{u}{\rho} + \eta_z D_\eta \frac{w}{\rho} - \frac{5}{3} \eta_z w D_\eta \frac{1}{\rho} - \frac{5}{3} \eta_z \frac{1}{\rho} \frac{\partial u}{\partial \eta} \right]$$

$$P_{53} = \mu \left[D_r \frac{v}{\rho} - \frac{2v}{\rho r} + \eta_\theta D_\eta \frac{w}{\rho} - \frac{5w}{3} \eta_\theta D_\eta \frac{1}{\rho} \right]$$

$$P_{54} = \mu \left[1.333 D_r \frac{w}{\rho} - \frac{4}{3} \frac{w}{\rho r} + \eta_\theta D_\eta \frac{v}{\rho} + \eta_z D_\eta \frac{u}{\rho} - \frac{5}{3} \eta_\theta \frac{1}{\rho} \frac{\partial v}{\partial \eta} \right]$$

D_r , D_η denote operators of the form $\frac{\partial}{\partial r} \left\{ \left(\frac{\partial q}{\partial \xi} \right) \right\}$, $\frac{\partial}{\partial \eta} \left\{ \left(\frac{\partial q}{\partial \xi} \right) \right\}$, respectively.

The Jacobian Matrix of the Vector \hat{Q}

$$q_{21} = -\left\{\mu(\eta_\theta^2 + \eta_z^2)D_\eta \frac{u}{\rho} + \frac{\mu}{3} \eta_z (\eta_\theta D_\eta \frac{v}{\rho} + \eta_z D_\eta \frac{u}{\rho}) - \frac{2}{3} \mu(D_r \frac{w}{\rho} + \frac{w}{\rho r})\right\}$$

$$q_{22} = \mu(\eta_\theta^2 + \frac{4}{3} \eta_z^2)D_\eta \left(\frac{1}{\rho}\right)$$

$$q_{23} = \frac{\mu}{3} \eta_\theta \eta_z D_\eta \left(\frac{1}{\rho}\right)$$

$$q_{24} = -\frac{2}{3} \mu(D_r \frac{1}{\rho} + \frac{1}{\rho r})$$

$$q_{31} = -\left\{\mu(\eta_\theta^2 + \eta_z^2)D_\eta \frac{v}{\rho} + \frac{\mu}{3} \eta_\theta (\eta_\theta D_\eta \frac{v}{\rho} + \eta_z D_\eta \frac{u}{\rho}) - \frac{2}{3} \mu(D_r \frac{w}{\rho} + \frac{w}{\rho r})\right\}$$

$$q_{32} = \frac{\mu}{3} \eta_\theta \eta_z D_\eta \frac{1}{\rho}$$

$$q_{33} = \mu(\eta_\theta^2 + \frac{4}{3} \eta_z^2)D_\eta \frac{1}{\rho}$$

$$q_{34} = -\frac{2}{3} \mu(D_r \frac{1}{\rho} + \frac{1}{\rho r})$$

$$q_{41} = -\left\{\mu(\eta_\theta^2 + \eta_z^2)D_\eta \frac{w}{\rho} + \mu(\eta_\theta D_r \frac{v}{\rho} - \eta_\theta \frac{v}{\rho r} + \eta_z D_r \frac{u}{\rho})\right\}$$

$$q_{42} = \mu \eta_z D_r \frac{1}{\rho}$$

$$q_{43} = \mu \eta_\theta \left\{D_r \frac{1}{\rho} - \frac{1}{\rho r}\right\}$$

$$q_{44} = \mu(\eta_\theta^2 + \eta_z^2)D_\eta \frac{1}{\rho}$$

$$q_{51} = \mu\left\{-\left(\eta_\theta^2 + \eta_z^2\right)D_\eta \frac{u^2 + v^2 + w^2}{\rho} - \frac{1}{6} \eta_\theta^2 D_\eta \frac{v}{\rho} - \eta_z^2 D_\eta \frac{u}{\rho} - 4\eta_\theta \eta_z D_\eta \frac{uv}{\rho} - \frac{8}{3} \frac{vw}{\rho r} + \frac{2}{3} \frac{v}{\rho} \frac{\partial w}{\partial r} - \frac{2vw}{\rho r^3} - w D_r \frac{w}{\rho} - \frac{w}{\rho} \frac{\partial v}{\partial r} + \frac{2}{3} u D_r \frac{w}{\rho} + \frac{2}{3} \frac{u}{\rho} \frac{\partial w}{\partial r} - w D_r \frac{u}{\rho} - \frac{w}{\rho} \frac{\partial u}{\partial r}\right\}$$

$$q_{52} = \mu\left\{\left(\eta_\theta^2 + 1.33 \eta_z^2\right) D_\eta \frac{u}{\rho} + 2\eta_\theta \eta_z D_\eta \frac{v}{\rho} - \frac{2}{3} \frac{1}{\rho} \frac{\partial w}{\partial r} + w D_r \frac{1}{\rho}\right\}$$

$$q_{53} = \mu\left\{\left(1.33 \eta_\theta^2 + \eta_z^2\right) D_\eta \frac{v}{\rho} + 2\eta_\theta \eta_z D_\eta \frac{u}{\rho} + \frac{4}{3} \frac{w}{\rho r} - \frac{2}{3} \frac{1}{\rho} \frac{\partial w}{\partial r} + \frac{w}{\rho r}\right\}$$

$$q_{54} = \mu \left\{ (\eta_{\theta}^2 + \eta_z^2) D_{\eta} \frac{w}{\rho} + \frac{4}{3} \frac{v}{\rho r} - \frac{2v}{3} D_r \frac{1}{\rho} + \frac{v}{\rho r^3} + w D_r \frac{1}{\rho} + \frac{1}{\rho} \frac{\partial v}{\partial r} \right. \\ \left. - \frac{2}{3} u D_r \frac{1}{\rho} + \frac{1}{\rho} \frac{\partial u}{\partial r} \right\}$$

The Jacobian Matrix of the Vector S

$$s_{21} = -\frac{\mu}{r} \left\{ D_r \frac{u}{\rho} + \eta_z D_\eta \frac{w}{\rho} \right\}$$

$$s_{22} = \frac{\mu}{r} D_r \frac{1}{\rho}$$

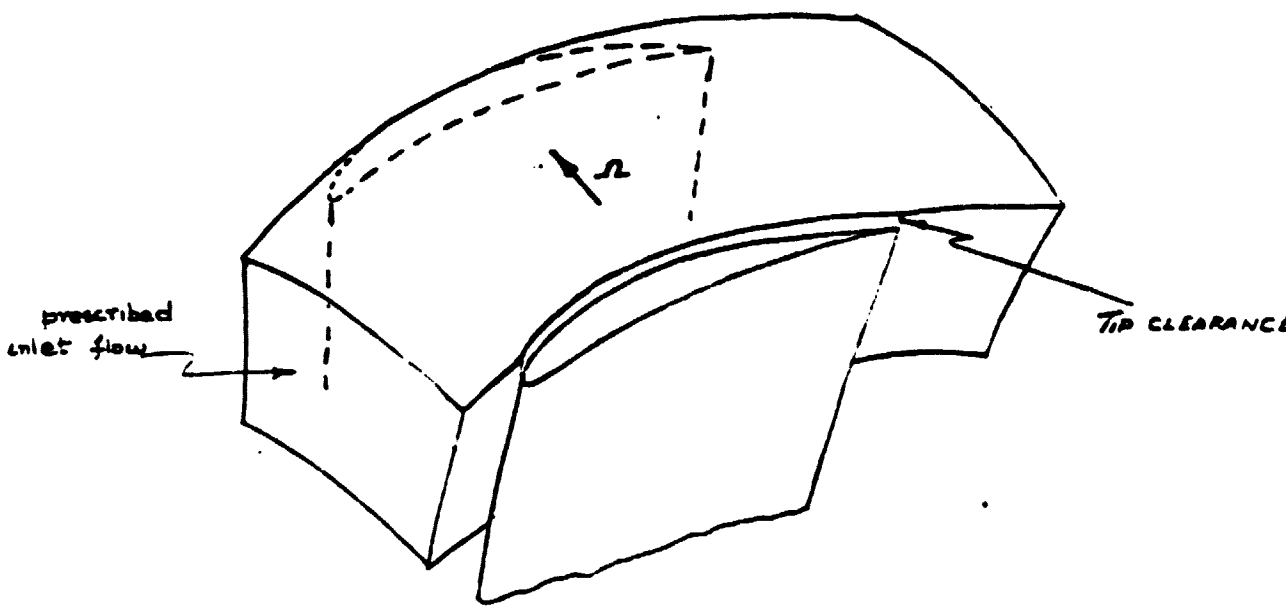
$$s_{24} = \frac{\mu}{r} \eta_z D_\eta \frac{1}{\rho}$$

$$s_{31} = -\frac{2\mu}{r} \left\{ \eta_\theta D_\eta \frac{w}{\rho} + D_r \frac{v}{\rho} - \frac{v}{\rho r} \right\}$$

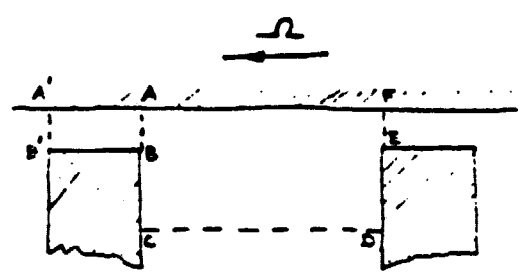
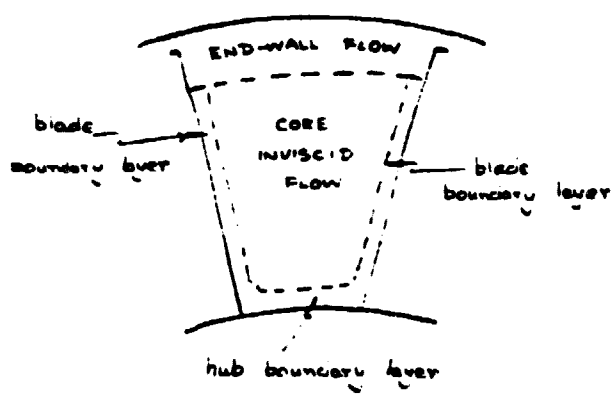
$$s_{33} = \frac{2\mu}{r} \left(D_r \frac{1}{\rho} - \frac{1}{\rho r} \right)$$

$$s_{34} = \frac{2\mu}{r} \eta_\theta D_\eta \frac{1}{\rho}$$

$$s_{41} = -\frac{2\mu}{r} \left\{ D_r \frac{w}{\rho} - \eta_\theta D_\eta \frac{v}{\rho} - \frac{w}{\rho r} \right\}$$



END-WALL FLOW DOMAIN



Section of the domain
(curvature neglected)

Relation of the end-wall flow
to the rest of the flow domain:

Fig. 1 Endwall Flow



ORIGINAL PAGE IS
OF POOR QUALITY

Figure 2. Two-Sensor Hot-Wire Probe

ORIGINAL PAGE IS
OF POOR QUALITY

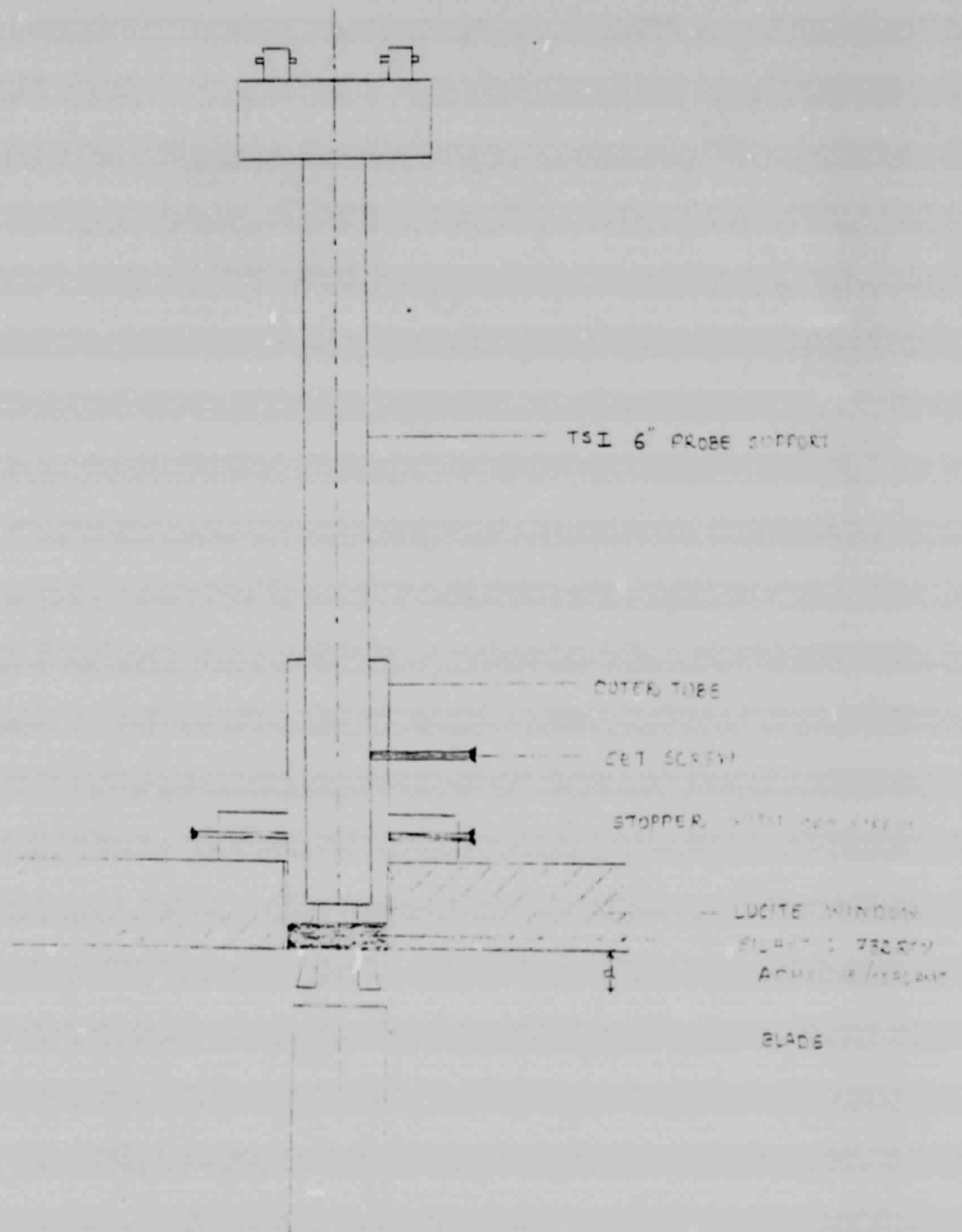
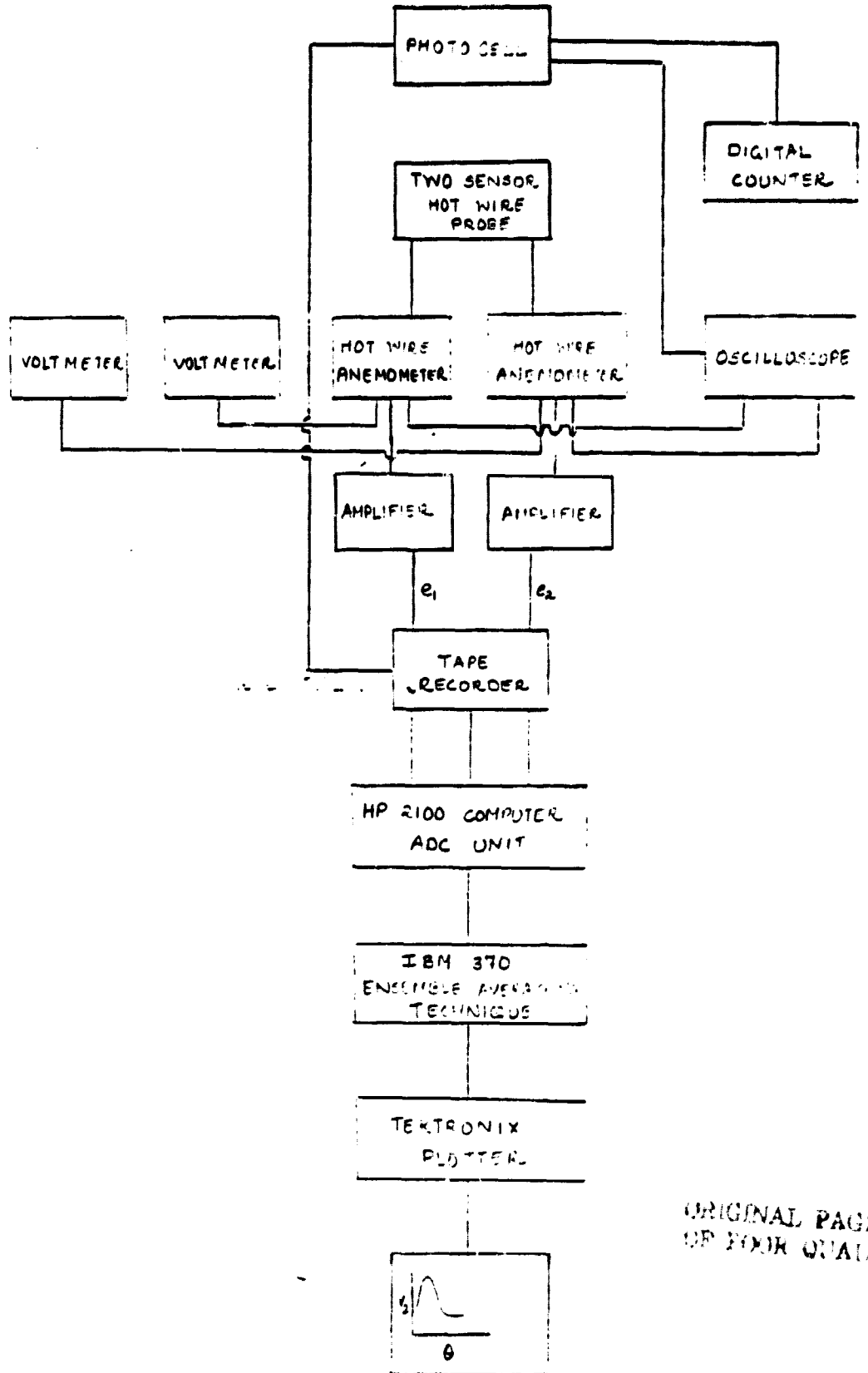


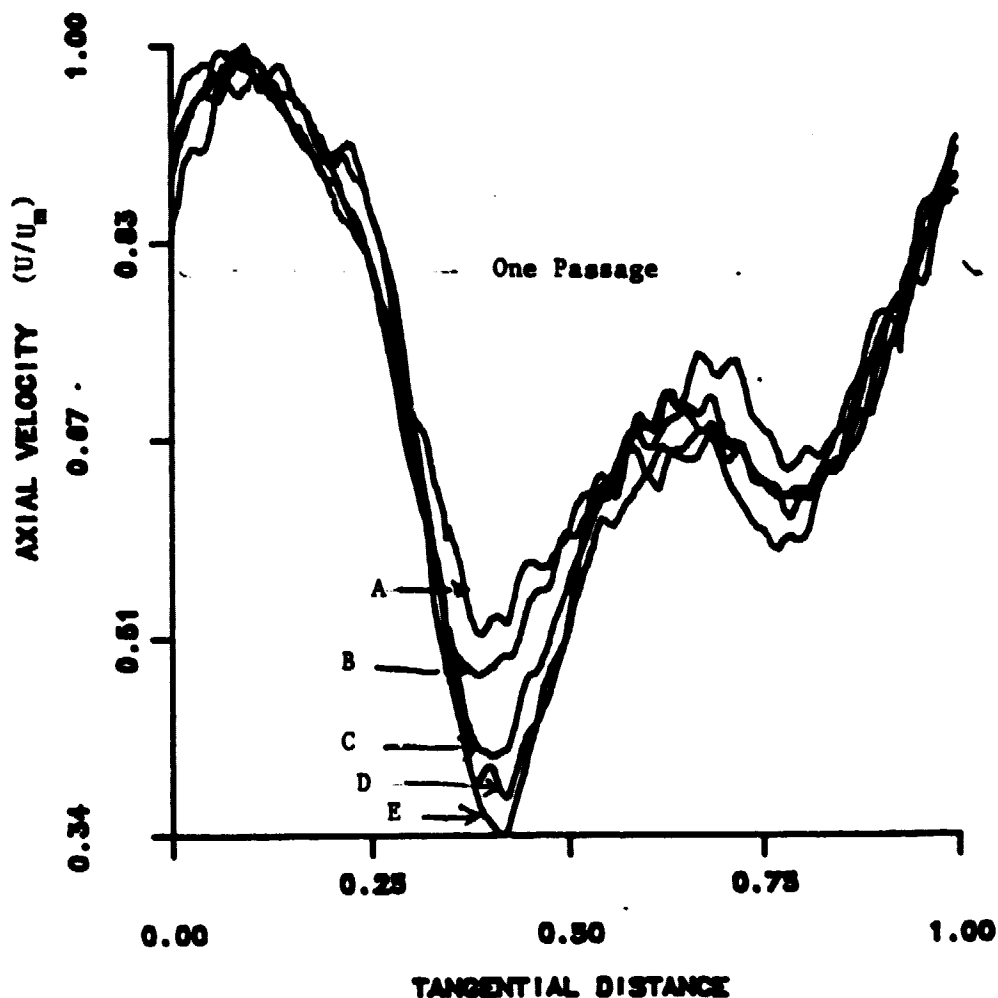
Figure 3. Probe Set-Up for Leakage Flow Measurement



ORIGINAL PAGE IS OF POOR QUALITY

Figure 4. Instrumentation for Hot Wire Measurements

VARIATION OF AXIAL VELOCITY

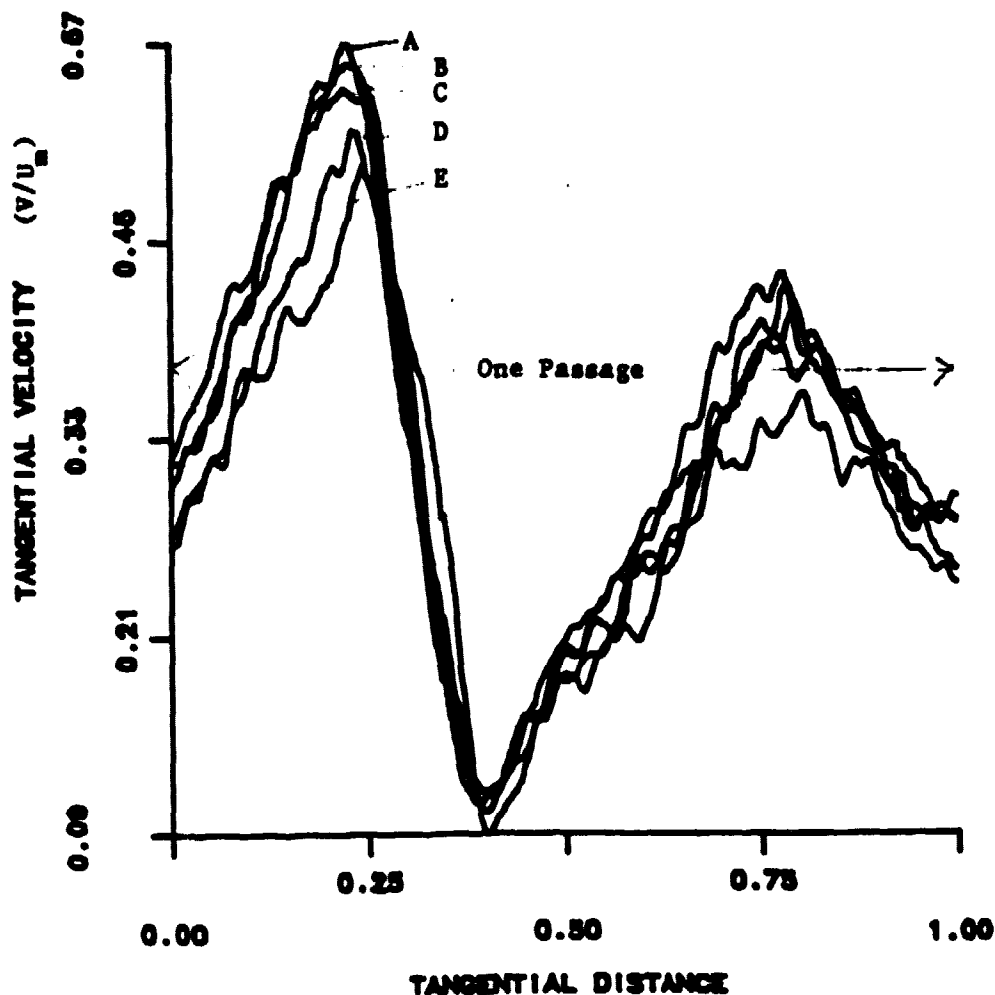


Radial Station

- A = 0.04" from the wall
- B = 0.035" from the wall
- C = 0.040" from the wall
- D = 0.025" from the wall
- E = 0.015" from the wall

Figure 5. Tangential Variation of Axial Velocity Inside the Gap at Various Radial Locations ($z/c = 0.75$, Tip Clearance Height 0.059" to 0.069")

VARIATION OF TANGENTIAL VELOCITY

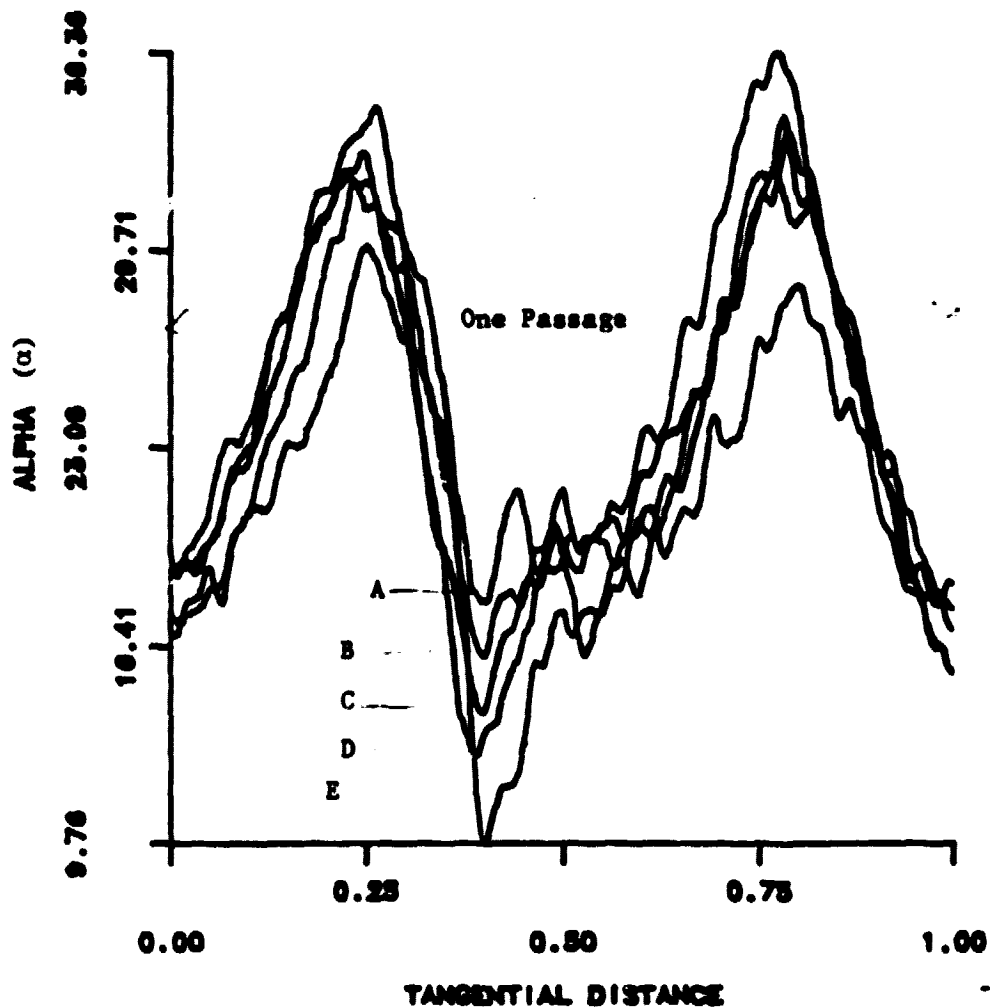


Radial Station

- A = 0.04" from the wall
- B = 0.035" from the wall
- C = 0.040" from the wall
- D = 0.025" from the wall
- E = 0.015" from the wall

Figure 6. Tangential Variation of Absolute Tangential Velocity Inside the Gap at Various Radial Locations ($z/c = 0.75$, Tip Clearance Height 0.059" to 0.069")

VARIATION OF ALPHA



Radial Station

- A = 0.04" from the wall
- B = 0.035" from the wall
- C = 0.040" from the wall
- D = 0.025" from the wall
- E = 0.015" from the wall

Figure 7. Tangential Variation of Absolute Angle Inside the Gap at Various Radial Locations ($z/c = 0.75$, Tip Clearance Height 0.059" to 0.069")

VARIATION OF MAXIMUM AXIAL VELOCITY IN RADIAL DIRECTION

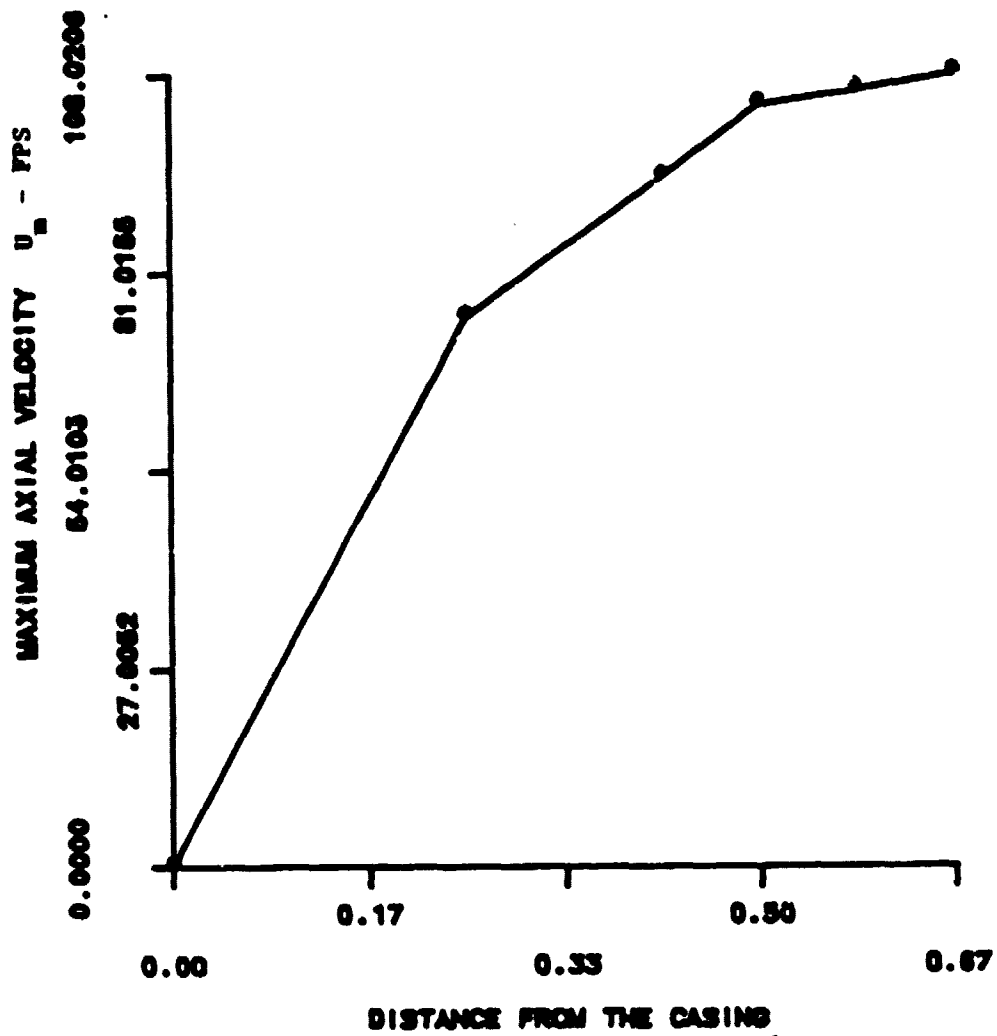
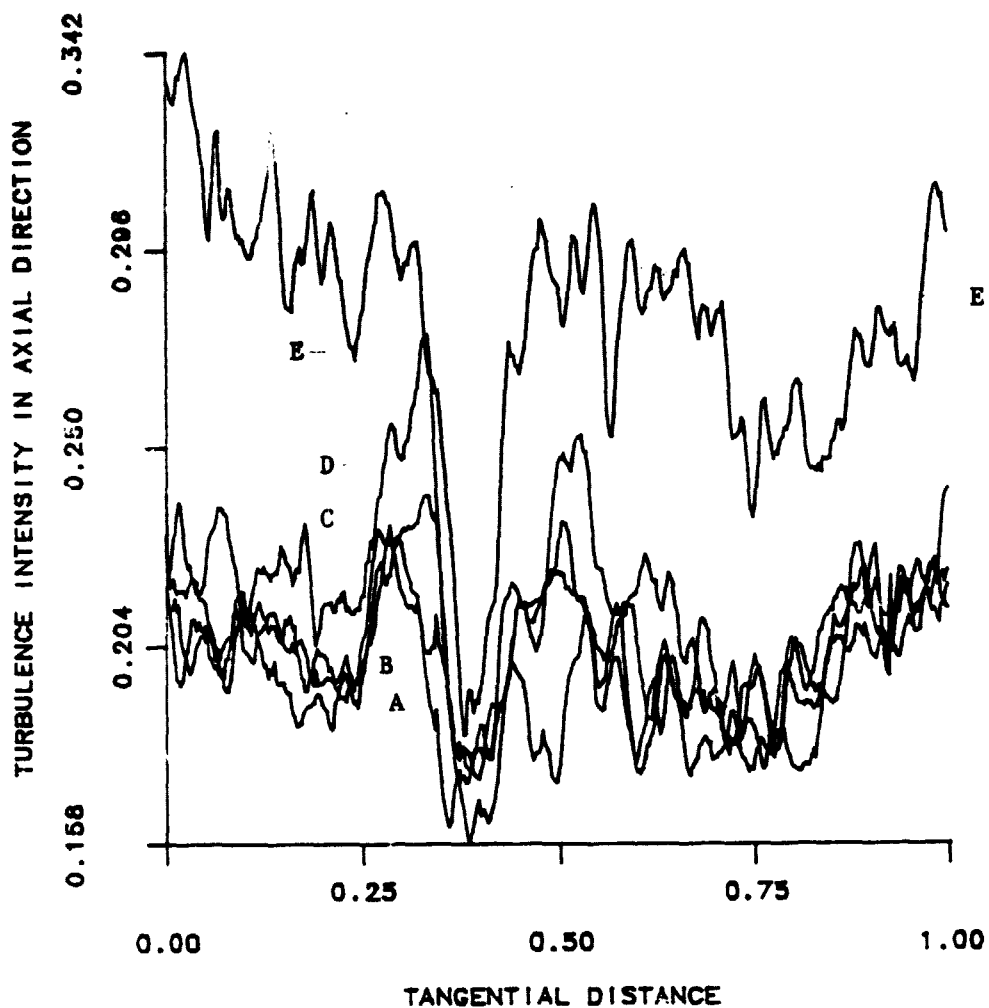


Figure 8. Radial Variation of Maximum Axial Velocity

VARIATION OF TURBULENCE INTENSITY IN AXIAL DIRECTION

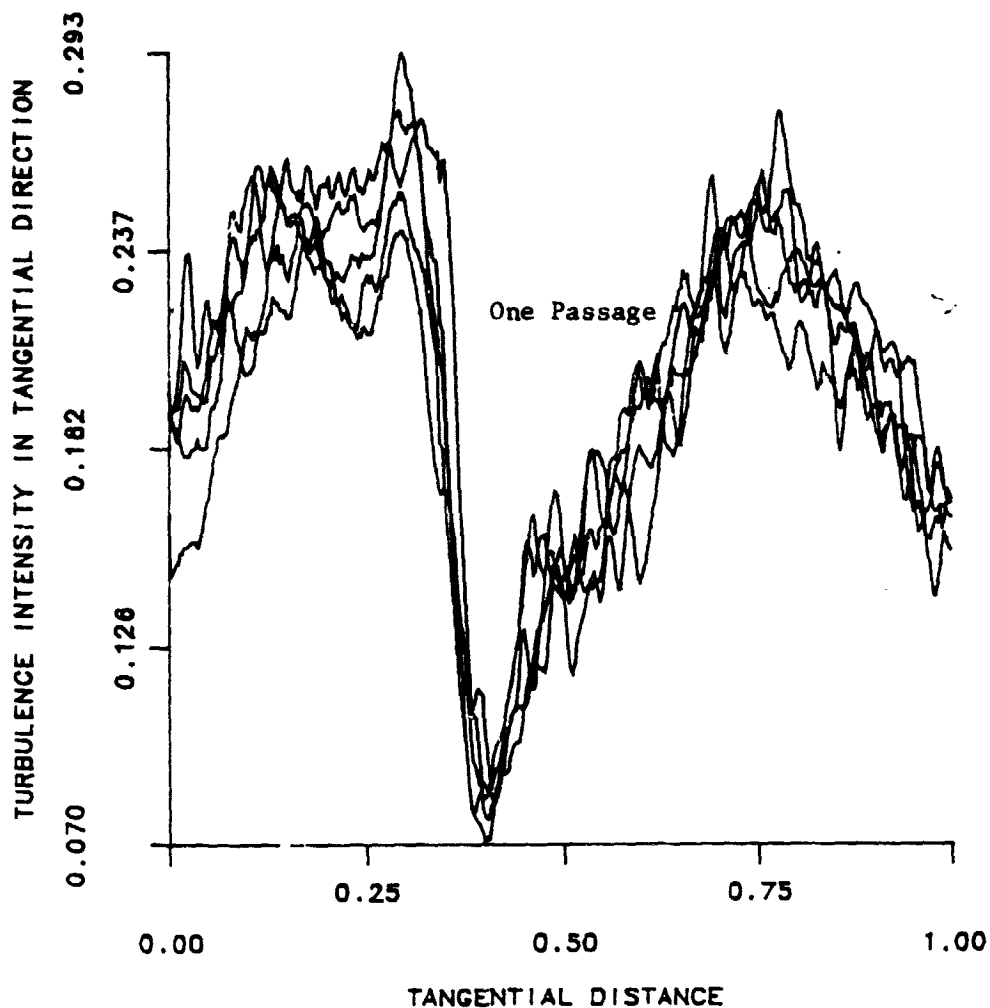


Radial Station

- A = 0.04" from the wall
- B = 0.035" from the wall
- C = 0.040" from the wall
- D = 0.025" from the wall
- E = 0.015" from the wall

Figure 9. Tangential Variation in Axial Turbulence Inside the Gap at Various Radial Locations ($z/c = 0.75$, Tip Clearance Height 0.059" to 0.069")

VARIATION OF TURBULENCE INTENSITY IN TANGENTIAL DIRECTION



Radial Station

- A = 0.04" from the wall
- B = 0.035" from the wall
- C = 0.040" from the wall
- D = 0.025" from the wall
- E = 0.015" from the wall

Figure 10. Tangential Variation of Axial Velocity Inside the Gap at Various Radial Locations ($z/c = 0.75$, Tip Clearance Height 0.059" to 0.069")

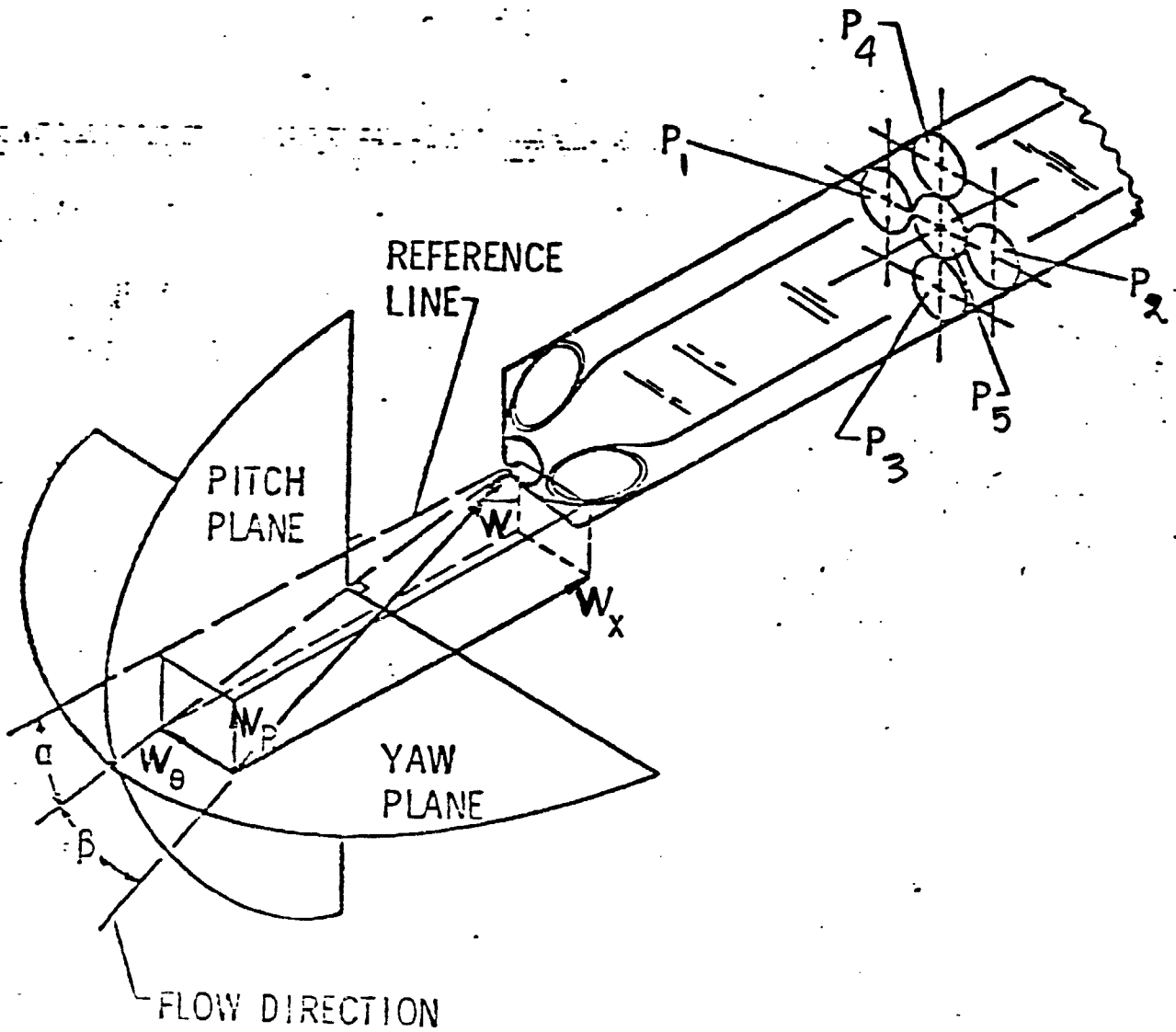


Fig.11 - GEOMETRY OF THE ANGLE-TUBE PROBES

ORIGINAL PAGE IS
OF POOR QUALITY

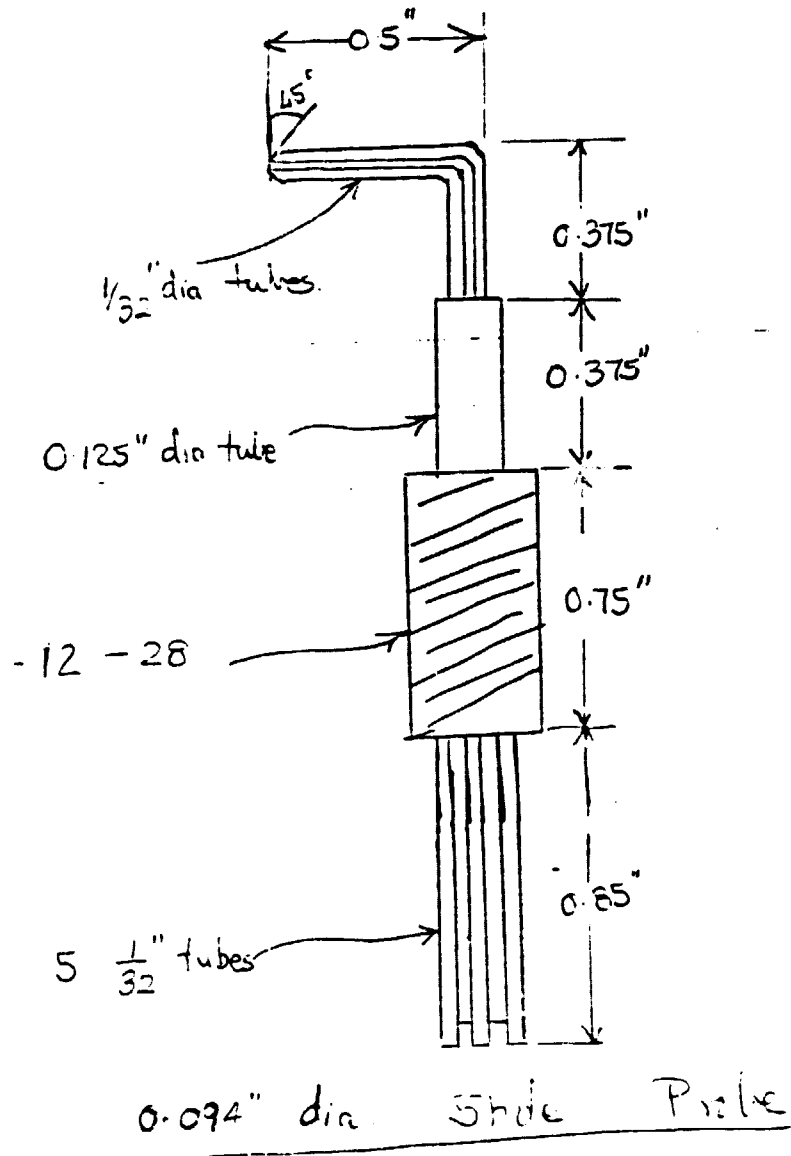
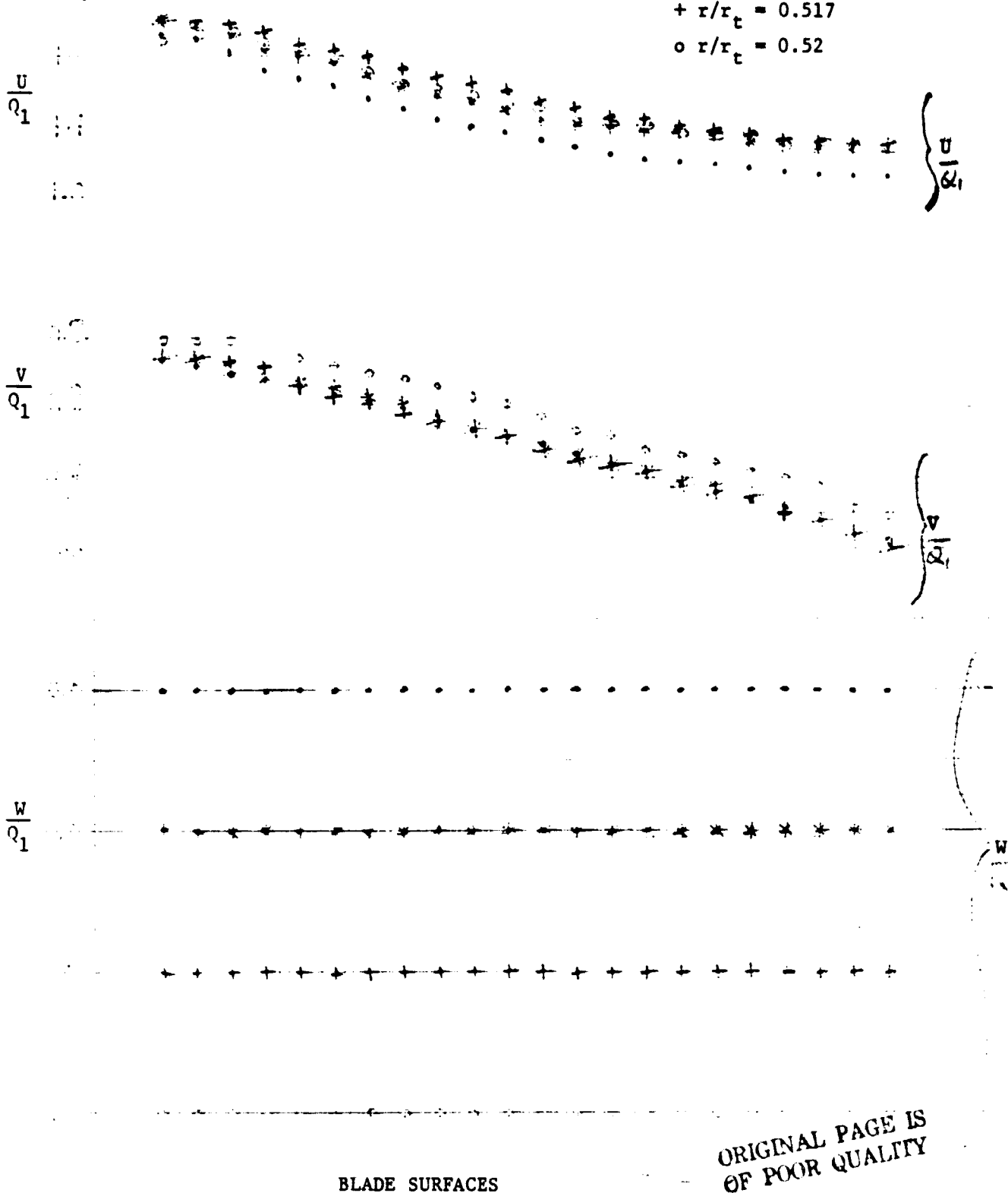


Figure 12. The Geometry of the Five-Hole Probe

- $r/r_t = 0.51$
- * $r/r_t = 0.5136$
- + $r/r_t = 0.517$
- o $r/r_t = 0.52$



ORIGINAL PAGE IS
OF POOR QUALITY

SS

PE

Figure 13. Blade to Blade Distribution of Axial, Tangential, and Radial Relative Velocity in the Hub Region at $z/c = 0.247$

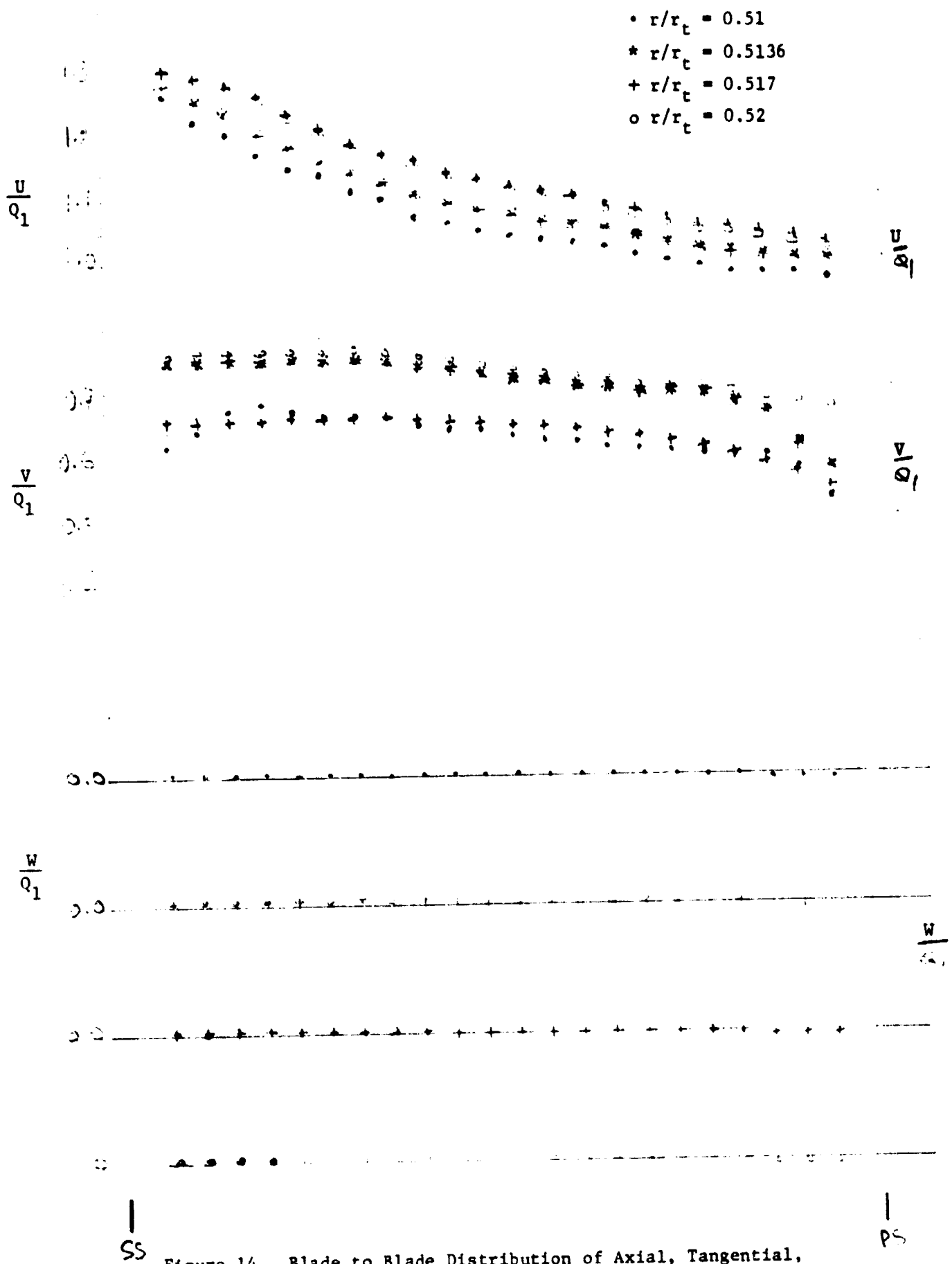
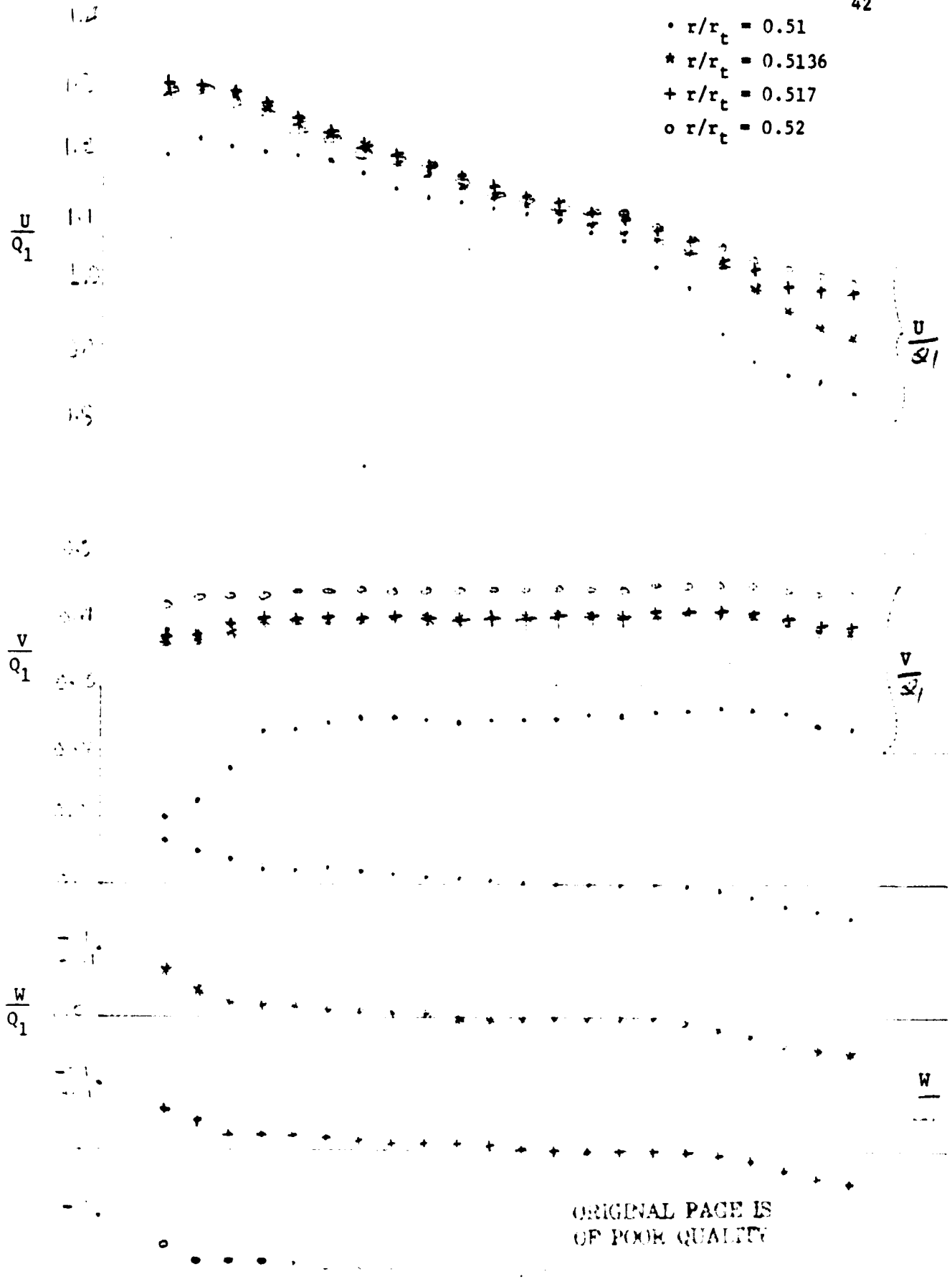
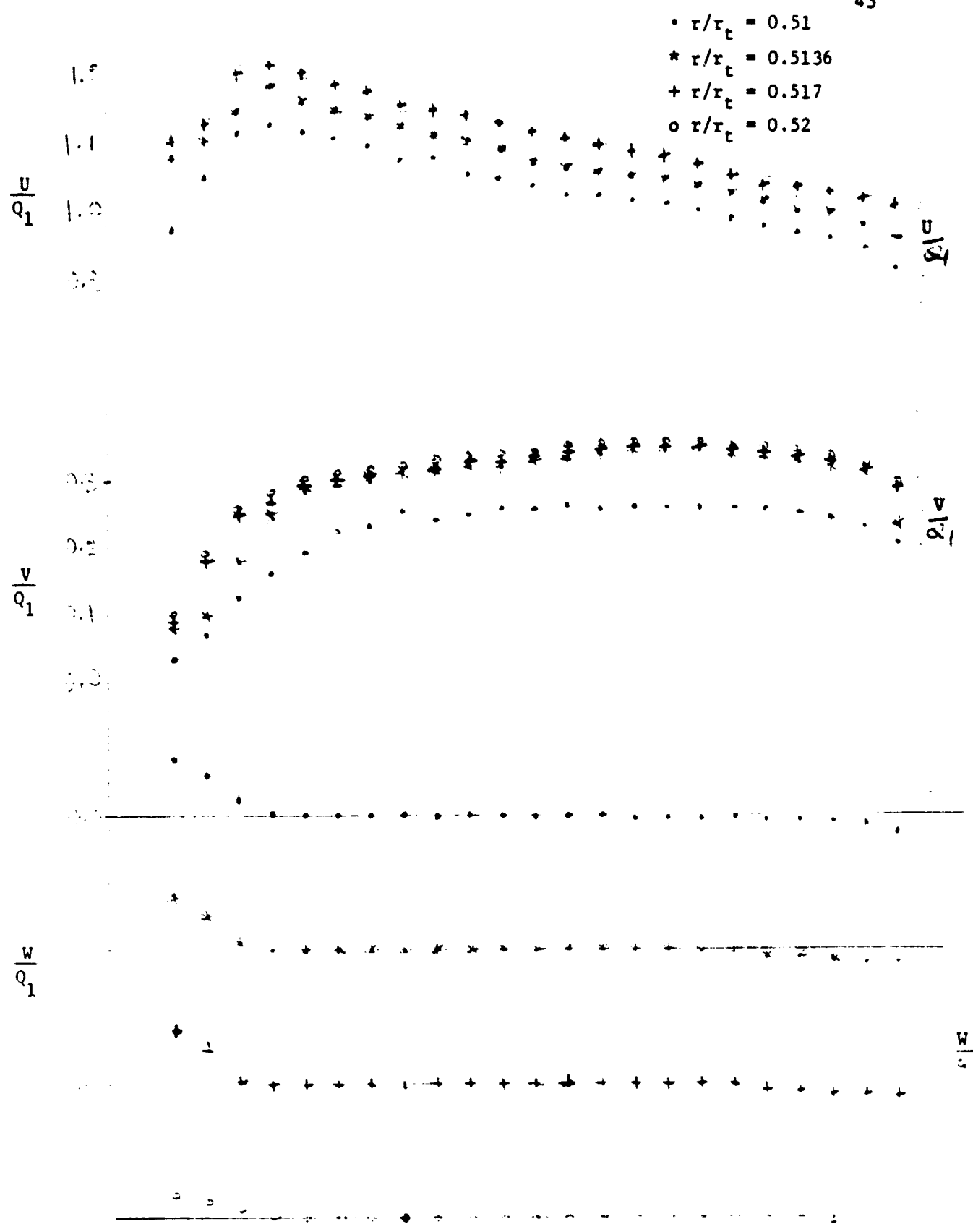


Figure 14. Blade to Blade Distribution of Axial, Tangential, and Radial Relative Velocity in the Hub Region at $z/c = 0.45$



SS | Figure 15. Blade to Blade Distribution of Axial, Tangential,
 and Radial Relative Velocity in the Hub Region at
 $\alpha/c = 0.66$

|
 PS



SS Figure 16. Blade to Blade Distribution of Axial, Tangential, and Radial Relative Velocity in the Hub Region at $z/c = 0.866$
PS

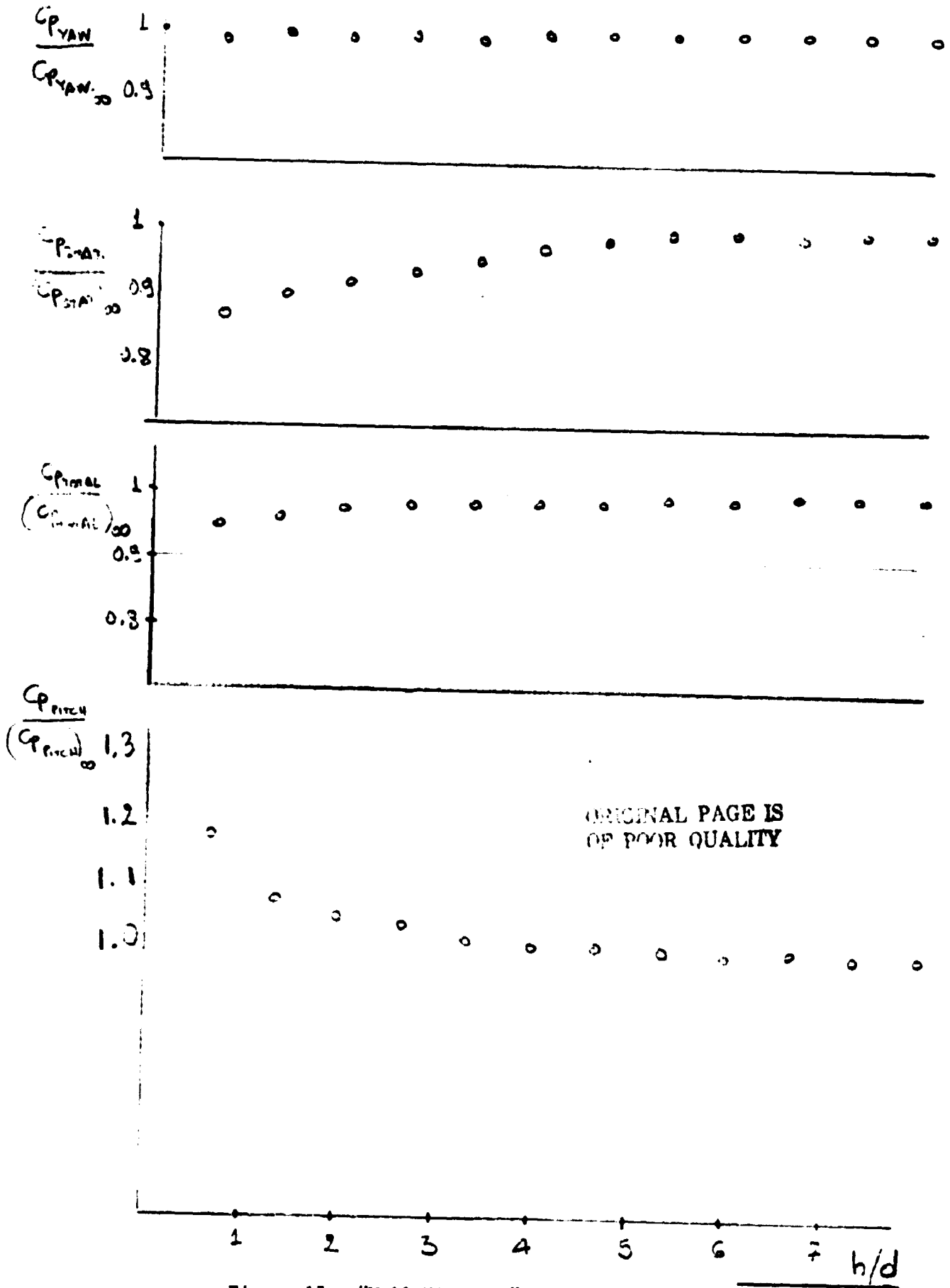


Figure 17. "Wall Vicinity" Effect